GERMAN - MONGOLIAN INSTITUTE FOR RESOURCES AND TECHNOLOGY

The present work was submitted to
the German-Mongolian Institute of Resources and Technology

SIMULATION-BASED STUDY OF HORIZONTAL AXIS WIND TURBINE BEHAVIOUR UNDER HARSH CLIMATIC CONDITIONS OF MONGOLIA

Bachelor's Thesis

By

ENKHJIN Batjargal

Study program: Mechanical Engineering

Student ID: B2200223

1st Supervisor/Examiner: Ph.D Sungchil Lee

2nd Supervisor/Examiner: Ph.D Gantuya Ganbat

Ulaanbaatar/Nalaikh

2026

GERMAN - MONGOLIAN INSTITUTE FOR RESOURCES AND TECHNOLOGY

The present work was submitted to
the German-Mongolian Institute of Resources and Technology

SIMULATION-BASED STUDY OF HORIZONTAL AXIS WIND TURBINE BEHAVIOUR UNDER HARSH CLIMATIC CONDITIONS OF MONGOLIA

Bachelor's Thesis

By

ENKHJIN Batjargal

Study program: Mechanical Engineering

Student ID: B2200223

1st Supervisor/Examiner: Ph.D Sungchil Lee

2nd Supervisor/Examiner: Ph.D Gantuya Ganbat

Ulaanbaatar/Nalaikh

2026

Statutory Declaration

Batjargal, Enkhjin B2200223

I hereby affirm in lieu of an oath that I provided the submitted bachelor thesis

SIMULATION-BASED STUDY OF HORIZONTAL AXIS WIND TURBINE BEHAVIOUR UNDER HARSH CLIMATIC CONDITIONS OF MONGOLIA

I did not use any sources other than those stated. In case that the work is additionally submitted on a data medium, I declare that the written and the electronic form are completely identical. The work was not submitted in the same or similar form to any examination authority.

Ulaanbaatar/Nalaikh, 2026/05/27

Place, Date

Signature

Abstract

Wind energy is a key part of Mongolia's transition to clean electricity, but the country's harsh climate raises questions about whether wind turbines designed for moderate regions can operate safely in winters that drop below -30°C s Celsius. This thesis investigates the fatigue behavior of a representative horizontal axis wind turbine blade made of glass-fiber reinforced polymer under such sub-zero conditions, using a chain of established simulation tools rather than physical testing.

The reference machine is the GE 1.6-100, the model already installed in the first commercial wind farm of Mongolia in Sergelen. Real wind speed data measured at the GMIT campus weather station were used as the input. The aerodynamic loads were obtained from a Blade Element Momentum solver written in Python, which produced the flapwise and edgewise root bending moments at every wind speed in the dataset. These bending moments were then applied to a finite element model of the blade in ANSYS Mechanical, where a static structural analysis and the built-in fatigue tool predicted the life of the laminate. Three temperature-dependent S-N curves of glass-fiber reinforced polymer extracted from the OPTIMAT BLADES database were used to compare the response at room temperature, at -40°C and at +60°C. A modal analysis combined with a Fast Fourier Transform of the wind speed signal completed the picture by evaluating the resonance risk of the blade.

The simulations show that, in dry isothermal conditions, the blade can sustain more than one hundred million cycles at the maximum flapwise bending moment, that fatigue performance is slightly better at -40°C than at room temperature, and that the spectral content of the wind at the natural frequencies of the blade remains below twenty-two percent of the dominant peak. These results form a baseline against which more complete future studies, including ice accretion, freeze-thaw cycles, dust erosion and a realistic internal blade structure, can be compared. The work supports the broader goal of replacing coal-fired electricity in Mongolia with reliable, properly engineered wind power.

Acknowledgements

I would like to express my sincere gratitude to my supervisors Prof. Dr. Sungchil Lee, and Prof. Dr. Gantuya Ganbat, who have guided me throughout the process. The final year of my studies was particularly demanding, as the sudden rise of health complications during the 7th semester added to the challenges of completing the thesis. Their continuous support made the completion of this work possible.

I would also like to extend my gratitude to my advisors Prof. Young Suk Kim and Mr. Sergey Zambalov. They have shown profound interest in my work and always made time for me to help with my work. My thesis touched on several areas of engineering that were new to me, requiring me to learn unfamiliar concepts and software from scratch. Thanks to them, these objectives were fulfilled successfully, especially Mr. Sergey Zambalov, who introduced me to ANSYS Student, a Computer Aided Engineering (CAE) software.

Lastly, instructors at GMIT and the friends I made there made an enormous indirect contribution to this work. The knowledge they have passed on and experiences they have shared throughout these last four years are truly invaluable.

Table of Contents

Abstract 1
Acknowledgements 5
Table of Contents ..... **Error! Bookmark not defined.**
1. Introduction 5
1.1. Climate change and the rise of wind energy 5
1.2. Energy situation and wind potential of Mongolia 6
1.3. Why the Mongolian climate matters for wind turbines 6
1.4. Importance of structural behavior and motivation for fatigue analysis 7
1.5. Aim and structure of the thesis 7
2. Literature review 8
2.1. Loads and failure modes of wind turbine blades 8
2.2. Fatigue concept and the S-N curve 10
2.3. Recent studies on fatigue analysis of wind turbine blades 11
2.3.1. S-N and linear damage rule approaches 11
2.3.2. Progressive damage and stochastic approaches 12
2.3.3. Finite element studies in commercial codes 12
2.4. Environmental effects on blade fatigue 13
2.4.1. Effect of temperature on composite laminates 13
2.4.2. Icing on wind turbine blades 14
2.4.3. Other environmental factors: hail, dust, lightning 15
2.5. Research gap and contribution of the present work 15
3. Methodology 16
3.1. Model selection and wind data collection 16
3.1.1. Wind turbine design 16
3.1.2. Airfoil 17
3.1.3. Weather data 18
3.2. Load calculation 19
3.2.1. Flapwise and edgewise bending moments 19
3.2.2. Blade element momentum (BEM) theory 20
3.2.3. BEM theory calculation using Python 22
3.3. Numerical Analysis 24
3.3.1. General features of ANSYS Mechanical 24
3.3.2. Concept of fatigue and the S-N curve 25

3.3.3. Simulation setup 27
3.3.4. Fast Fourier Transform of the wind speed signal 29
3.4. Analysis assumptions 30
4. Results and discussion 32
4.1. Selection of the element size 32
4.2. Fatigue analysis 35
4.2.1. Fatigue results at different temperatures 38
4.3. Vibration analysis 43
4.3.1. Modal analysis 43
4.3.2. FFT of the wind speed signal 44
4.3.3. Resonance risk assessment 44
4.4. Limitations of the study and hypotheses 45
5. Conclusion 49
6. References 1
Appendix 4

List of Figures

Figure 1. Effect of Energiewende on Germany's CO2 emission [2] 5
Figure 2. Salkhit Wind Farm in Sergelen soum, Tuv province, Mongolia [3] 6
Figure 3. Blade cross section and aerodynamic forces [11] 8
Figure 4. Trailing edge and outer skin debonding [11] 9
Figure 5. Leading-edge erosion [19] 9
Figure 6. Wear due to lightning strike [19] 10
Figure 7. Ice accretion on wind turbine blade [19] 10
Figure 8. Example S-N curve or Wöhler diagram [11] 11
Figure 9. GFRP at temperatures of -25, 0, 25, 50, 75, 100°C [9] 14
Figure 10. (c) flexural strength and flexural strain at break, and (d) specific energy absorption per volume. [10] 14
Figure 11. GE 1.6-100 wind turbine 17
Figure 12. Cross section of NACA 4412 airfoil. Normally the coordinates are given, so that the geometry can be scaled. 18
Figure 13. Weather station at GMIT campus 18
Figure 14. S-N curve of GFRP at different environmental conditions extracted from OptiDAT database [15] 28

Figure 15. Model installed from GrabCAD community repository and loading direction 29
Figure 16. S-N curve of GFRP at room temperature and its trendline [15] 31
Figure 17. Element-quality histogram for an element size of 1 m 33
Figure 18. Element-quality histogram for an element size of 0.375 m 34
Figure 19a. Fatigue analysis result for a zero-based maximum flapwise bending moment 35
Figure 20a. Flapwise bending load history 36
Figure 21a. Fatigue result under flapwise operational loading 37
Figure 21b.
Figure 22a. Fatigue contour of zero-based flapwise bending of the GFRP blade at room temperature 39
Figure 23. FFT spectrum of the wind speed signal 44

List of Tables

Table 1. Necessary specifications of GE 1.6 - 100 wind turbine 16
Table 2. Static and fatigue results obtained at different element sizes 32
Table 3. Element-quality statistics at the smaller mesh sizes 34
Table 4. Natural frequencies of the first six modes 43
Table 5. Resonance risk assessment at the bins closest to the natural frequencies ... 45

List of Equations

Equation 1. Flapwise bending moment 19
Equation 2. Edgewise bending moment 19
Equation 3. Axial Thrust on the wind turbine 20
Equation 4. Resulting torque on the wind turbine shaft 20
Equation 5. Relative wind speed 21
Equation 6. Lift force applied on the airfoil 21
Equation 7. Drag force applied on the airfoil 21
Equation 8. Equation for coefficient "a" 21
Equation 9. Equation for coefficient " a' " 21
Equation 10. Basquin relation 26
Equation 11. Relation including the slope of the S-N curve "k" 26
Equation 12. Miner's rule 27

Equation 13.Fast Fourier Transform of X[n] discrete signal 29
Equation 14. Hanning window 29
Equation 15. Magnitude of the resulting complex number 30
Equation 16. Corresponding frequency 30

1. Introduction

1.1. Climate change and the rise of wind energy

Climate change has become one of the defining challenges of the present century. Although natural drivers such as solar variability and volcanic eruptions have caused large climatic shifts in the geological past, the changes observed since the 1800s, which coincide with the industrial revolution, are dominated by human activity. The mean temperature of the Earth's surface is now about 1.34°C to 1.41°C higher than the pre-industrial baseline, and the rising cost and environmental impact of fossil fuels are pushing every major economy to look for cleaner alternatives [1]. Wind energy, which is renewable, abundant and free at the point of generation, has emerged as one of the most attractive options.

Germany is often cited as a model for this transition. Its long-term policy known as the Energiewende was launched in the late twentieth century and has installed nearly 30 000 wind turbines, both onshore and offshore, that today produce around 32% of the country's net electricity [2]. As shown on Fig.1 Over a span of about forty years, this development has helped reduce the national carbon dioxide emissions from approximately 1.1 billion tons to 600 million tons, demonstrating that a large industrial economy can decarbonize while keeping its electricity supply stable.

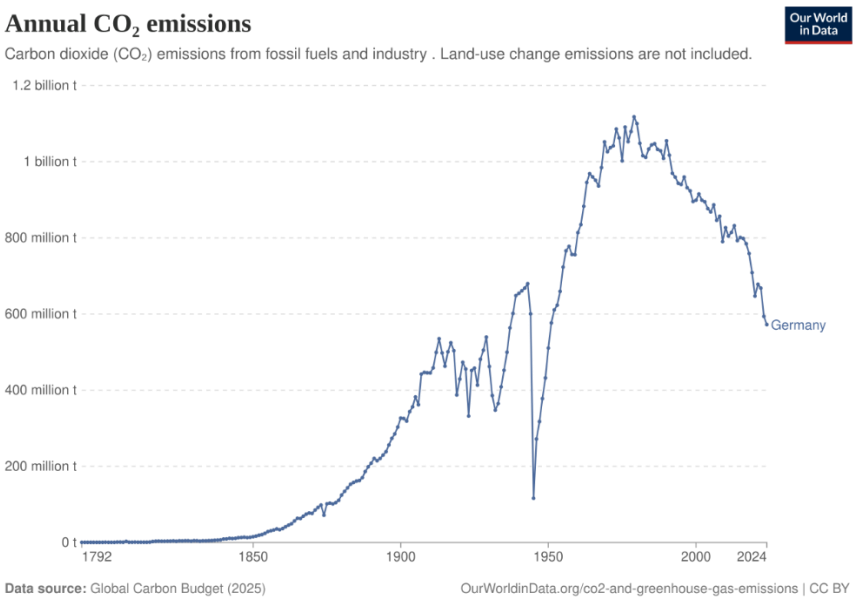


Figure 1. Effect of Energiewende on Germany's CO2 emission [2]

1.2. Energy situation and wind potential of Mongolia

Mongolia is in a very different position. The country holds about 0.2% of the global coal reserves, equivalent to roughly 165 billion tons, and approximately 87% of its electricity is currently produced from coal-fired power plants [3, 4]. The combustion of coal not only emits greenhouse gases but also contributes to severe wintertime air pollution in Ulaanbaatar, which has direct consequences for public health. Reducing the share of coal in the national electricity mix is therefore both a climate and a public-health priority.

Fortunately, Mongolia is not poor in renewable resources. The country lies on a high-altitude plateau between Siberia and the Gobi Desert, and its steppes and southern regions are exposed to strong and persistent winds. According to the Global Wind Atlas [5], the south-eastern part of Mongolia has a mean wind power density of about 505 W/m^2 in the windiest 10% of the area, which exceeds the 463 W/m^2 reported for the windiest 10 % of northern Germany. The first commercial wind farm in the country (Fig.2), located in Sergelen soum of Tuv province about 75 km south of Ulaanbaatar, was commissioned in 2013 and consists of 31 turbines of 1.6 MW each. Several additional projects have followed, but the installed capacity remains far below what the natural resources would allow.



Figure 2. Salkhit Wind Farm in Sergelen soum, Tuv province, Mongolia [3]

1.3. Why the Mongolian climate matters for wind turbines

Wind turbines designed for moderate climates cannot simply be copied to Mongolia and expected to perform as advertised. The country's climate is one of the most severe at its latitude: winter temperatures regularly fall below -30°C and extreme values of -40°C are

not unusual; daily temperature variations of 20°C or more between day and night are common in spring and autumn; dust storms in the Gobi region carry abrasive particles that can erode the leading edge of the blades; and short periods of icing occur whenever supercooled droplets impact a cold blade surface. Each of these factors modifies either the aerodynamic loading on the rotor, the mechanical properties of the composite material, or both [6, 7, 8, 9, 10]. A careful, site-specific evaluation of the structural behavior of the wind turbine is therefore necessary if the country wants to deploy wind energy in a safe and economically reliable manner.

1.4. Importance of structural behavior and motivation for fatigue analysis

Among all the parts of a wind turbine, the rotor blades are the most exposed and the most expensive single structures of the machine [11]. They must withstand many millions of load cycles over a service life of about twenty years, while operating in continuously changing wind conditions. Knowing how such a structure behaves, how it accumulates damage cycle after cycle, is therefore one of the most important parts of the design process. For modern multi-megawatt blades made of glass-fiber reinforced polymer, fatigue rather than static strength is the dominant failure driver, and any reliable life prediction must combine an aerodynamic load calculation with a fatigue analysis of the laminate [11, 12, 13]. For this reason, the present thesis is centered on a fatigue analysis of a representative HAWT blade under the sub-zero conditions of central Mongolia.

1.5. Aim and structure of the thesis

The aim of this work is to establish a baseline simulation of how a typical multi-megawatt GFRP wind turbine blade behaves, in fatigue, under the dry sub-zero conditions of central Mongolia, and to compare the results with the published literature. The reference machine is the GE 1.6-100; the model used in the Sergelen wind farm. Real wind data measured at the GMIT campus weather station serve as input to a Blade Element Momentum solver implemented in Python, which produces the flapwise and edgewise root bending moments. These loads are then applied to a finite element model of the blade in ANSYS Mechanical, and the fatigue tool is used together with three temperature-dependent S-N curves of GFRP extracted from the OPTIMAT BLADES OptiDAT database [14, 15] to predict the fatigue life at room temperature, at -40°C and at +60°C. A modal analysis combined with a Fast Fourier Transform of the wind signal completes the picture by evaluating the resonance risk of the blade.

The thesis is organized as follows. Chapter 2 reviews the literature on fatigue analysis of wind turbine blades and on the environmental effects on blade behavior. Chapter 3 describes the methodology, including the reference model, the BEM calculation, the FFT procedure and the ANSYS finite element setup. Chapter 4 reports and discusses the results of the mesh study, the fatigue analysis, the temperature comparison and the resonance assessment. Further it summarizes the limitations of the study and formulates seven hypotheses for further work in Mongolian conditions. Chapter 5 closes the thesis with a conclusion that frames the present work as a baseline for future, more refined studies of wind turbine reliability in the country.

2. Literature review

2.1. Loads and failure modes of wind turbine blades

Wind turbine blades are slender, twisted and tapered composite structures that are loaded by aerodynamic, gravitational, inertial and operational forces [11, 16]. Aerodynamic loads result from the lift and drag forces (Fig.3) along the span and are highly time-varying because of wind shear, atmospheric turbulence, yaw misalignment and tower shadow [16, 17]. Gravitational loads create a once-per-revolution edgewise bending moment that fully reverses every rotation, while centrifugal forces and operational events, namely being start-up, shutdown, pitching, and braking, add further inertial contributions. The combination produces a wide-band fluctuating stress field and places blades firmly in the high-cycle fatigue regime [11, 16].

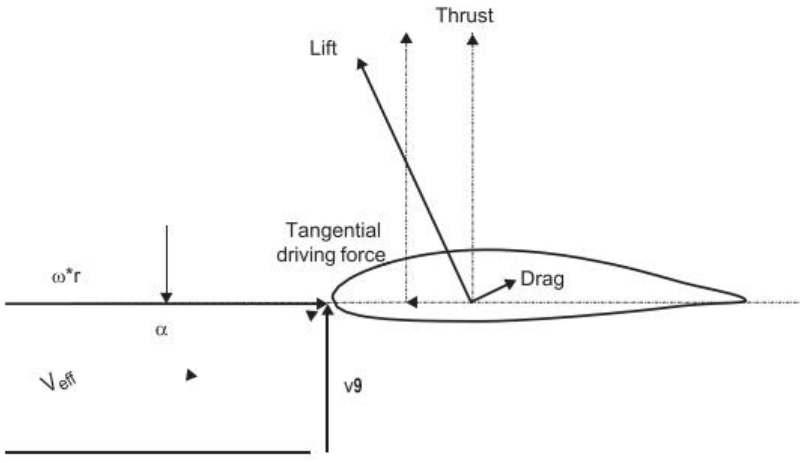


Figure 3. Blade cross section and aerodynamic forces [11]

Olabi et al. [18] reviewed the failure modes of wind turbine components and concluded that the rotor blades are responsible for the largest share of long downtimes, mainly because of the difficulty of replacing them. Katsaprakakis et al. [19] grouped the reported damage cases into structural, material, manufacturing, environmental and operational categories. Chou et al. [20] analyzed an actual blade failure that occurred under typhoon-level winds and confirmed that excessive flapwise bending produced delamination and final fracture near the root. The most frequently reported damage modes are trailing edge debonding, skin or spar cap debonding (Fig.4), leading-edge erosion (Fig.5), lightning damage (Fig.6), ice-related failures (Fig.7) and fatigue cracking of the laminate [11, 18, 19, 20].

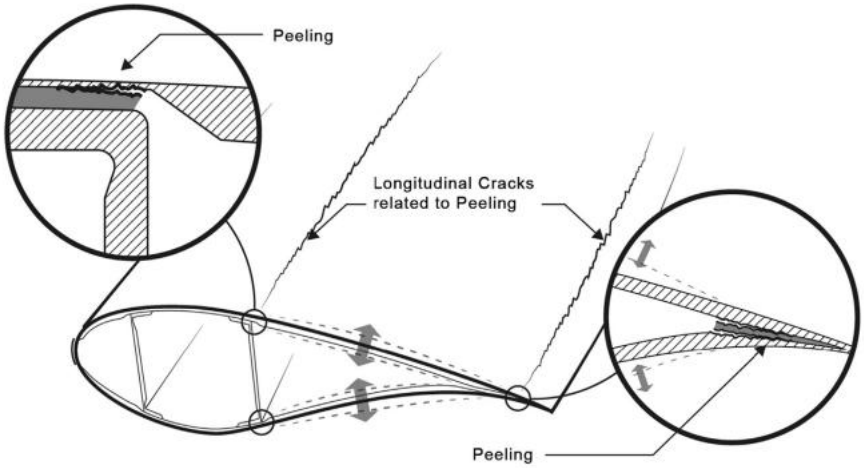


Figure 4. Trailing edge and outer skin debonding [11]



Figure 5. Leading-edge erosion [19]

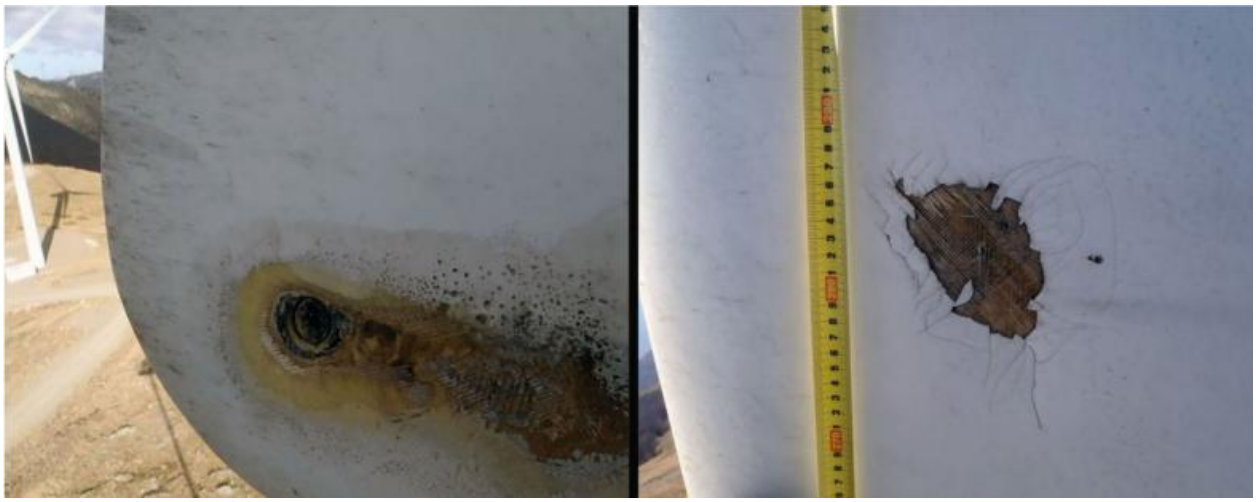


Figure 6. Wear due to lightning strike [19]



Figure 7. Ice accretion on wind turbine blade [19]

2.2. Fatigue concept and the S-N curve

Fatigue is the gradual weakening and final fracture of a material that is subjected to many cycles of fluctuating stress, even when the maximum stress is well below the static strength [21]. For metals, the boundary between high-cycle and low-cycle fatigue is conventionally placed near 10 to the 4 - 10 to the 5 cycles, but wind turbine blades typically experience between 10 to the 8 and 10 to the 9 cycles in twenty years and lie almost entirely in the high-cycle regime [11, 12]. The Wohler diagram, or S-N curve (Fig.8), plots the stress amplitude against the number of cycles to failure on a logarithmic scale. For composites no clear endurance limit is observed, and the curve is usually fitted with a power law or with Basquin's relation [12, 21].

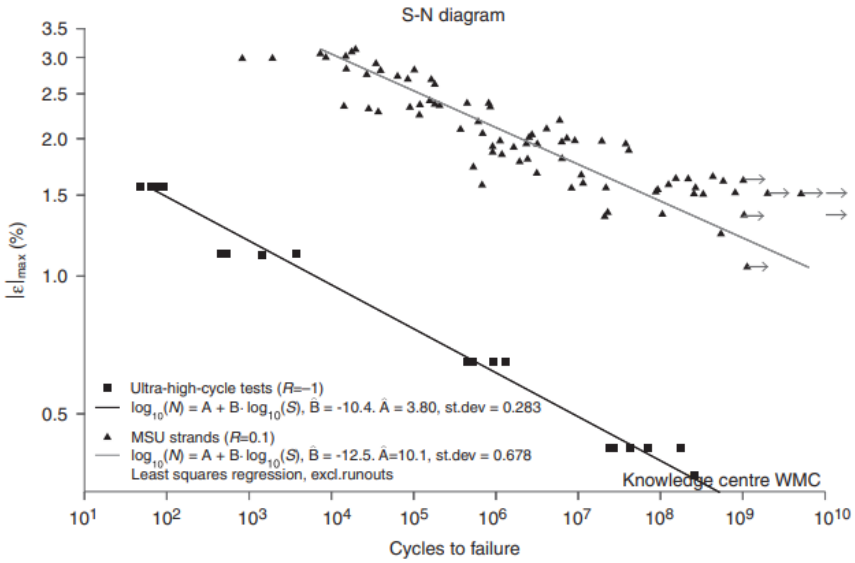


Figure 8. Example S-N curve or Wöhler diagram [11]

Damage in composite laminates is fundamentally different from damage in metals. Rather than propagating from a single dominant crack, it accumulates as a distributed network of matrix microcracks, fiber or matrix debonding and delamination, and the residual stiffness is often used as a more reliable indicator of damage than crack length [12, 22, 23]. For variable-amplitude loading, the linear Palmgren-Miner rule is the most widely used cumulative damage law, and design standards such as IEC 61400-1 still rely on it because of its simplicity [21].

2.3. Recent studies on fatigue analysis of wind turbine blades

Numerical fatigue analysis of composite wind turbine blades has been a very active research area for the past two decades. The studies can be grouped into three families according to the modelling approach.

2.3.1. S-N and linear damage rule approaches

The S-N curve combined with the linear Palmgren-Miner rule is the simplest and most widely used method for blade fatigue analysis. Kong et al. [13] presented a detailed structural design of a 750 kW E-glass/epoxy blade for the GL-rated load cases of the IEC 61400-1 standard. Using the S-N approach, Spera's empirical formulae and the operational load spectrum, they predicted a fatigue life longer than the 20-year design target and demonstrated the suitability of the method for industrial design when reliable S-N data are available. Kong et al. [24] later extended this work to a medium-scale blade

and confirmed that the linear damage rule provides adequate life predictions when the input loads cover the full operating envelope. Tawade et al. [25] applied the same approach in ANSYS to optimize the chord length, blade length and twist angle for maximum fatigue life. Their parametric study showed that the predicted life is highly sensitive to the local mesh refinement at the root, where the bending stresses concentrate.

2.3.2. Progressive damage and stochastic approaches

The linear damage rule has well-known limitations. It does not account for load-sequence effects, mean-stress dependence or interaction between damage modes, all of which are important for composites [12, 23]. To address these issues, several authors developed progressive damage and stochastic approaches. Shokrieh and Rafiee [26] performed a full three-dimensional finite element simulation of a composite blade under stochastic wind loads weighted by the Weibull distribution. Their accumulated damage model gradually degraded the local material properties of every laminate ply during the simulation and reproduced realistic failures at the spar cap and at the root. The predicted lives were significantly shorter than those obtained with the linear rule, suggesting that S-N-based predictions tend to be optimistic. Colombo et al. [23] complemented these numerical works with extensive coupon tests on cross-ply E-glass/epoxy and showed that the stiffness reduction during fatigue can be modelled as a smooth function of the cycle ratio n/N, which provides a useful link between coupon-level data and blade-level life prediction.

Two large international research programmes underpin all these approaches. The European OPTIMAT BLADES project, run between 2002 and 2006, generated extensive static and fatigue data on a representative E-glass/epoxy laminate at several R-values, mean stress and temperatures [14]. The SNL/MSU/DOE Composite Material Fatigue Database, developed jointly by Sandia National Laboratories, Montana State University and the U.S. Department of Energy, complements OPTIMAT with results on a wider range of glass and carbon laminates and is updated continuously [27]. The PhD thesis of Nijssen [12] is one of the most cited works in the field and provides constant-life diagrams that allow tests at one R-value to be converted into design curves for any other R-value.

2.3.3. Finite element studies in commercial codes

In recent years, the increasing maturity of commercial finite element codes such as ANSYS, ABAQUS and Bladed has made high-fidelity blade simulations accessible to a

wide community. Tawade et al. [25] used the ANSYS fatigue tool with Morrow's mean-stress correction to predict the fatigue life of a GFRP blade and to study how chord length, blade length and twist angle influence it. Navadeh et al. [28] performed a finite element modal analysis of a HAWT blade in ABAQUS and obtained natural frequencies very close to those observed in the present work, with the first flapwise mode near 0.27 Hz. Their study also highlighted the importance of mesh independence: a coarse mesh shifted the natural frequencies by several percent and changed the mode shapes in the higher modes. The combination of S-N data from the OPTIMAT or SNL/MSU/DOE databases [14, 15, 27] with finite element analysis in ANSYS Mechanical, as adopted in the present thesis, is therefore a well-established methodology that allows the engineer to explore design variations and operating conditions at a moderate computational cost.

2.4. Environmental effects on blade fatigue

Beyond the structural loads, the environment in which a wind turbine operates strongly influences the fatigue behavior of the blade. Three families of environmental effects are particularly relevant for Mongolia: temperature, icing and surface erosion or impact damage.

2.4.1. Effect of temperature on composite laminates

The mechanical properties of GFRP and CFRP depend strongly on temperature, mainly because the polymer matrix becomes stiffer and more brittle at low temperatures and softer at high temperatures. Ou et al. [9] tested unidirectional E-glass/epoxy specimens at six temperatures between -25°C and 100°C and reported a clear increase of tensile strength and Young's modulus when the temperature decreased, with strength gains of about 15 % between 25°C and -25°C (Fig.9). The strain to failure decreased over the same range, confirming the brittle character of the matrix at low temperatures. Jia et al. [10] performed three-point bending tests on CFRP between -100°C and 100°C. As shown on Fig.10, the study found a similar trend: the flexural strength and the energy absorbed before failure both increased as the temperature was lowered, until brittle behavior started to dominate below about -60°C. Both studies attribute the favorable cold-temperature response to the matrix becoming stiffer and the fiber or matrix interface becoming tighter.

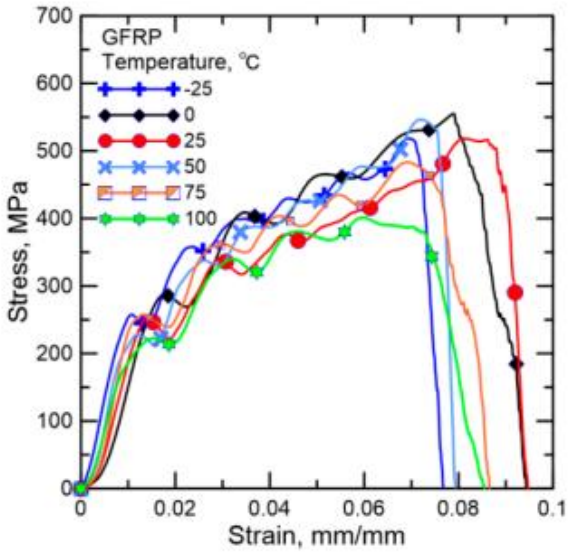


Figure 9. GFRP at temperatures of -25, 0, 25, 50, 75, 100°C [9]

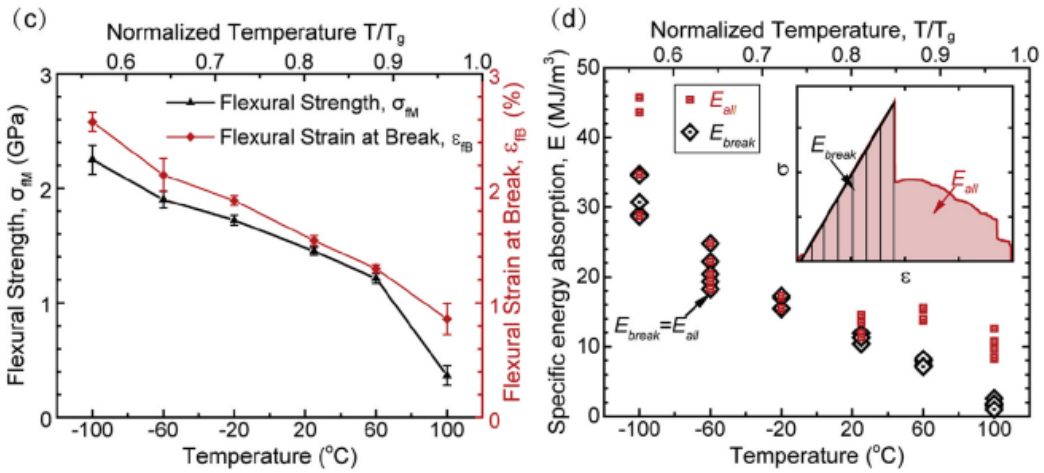


Figure 10. (c) flexural strength and flexural strain at break, and (d) specific energy absorption per volume. [10]

The OPTIMAT BLADES project [14, 15] also produced fatigue data at several temperatures, on which the present simulations are based. The general picture from these works is that, for fiber dominated longitudinal properties, the laminate becomes stronger and stiffer at sub-zero temperatures, whereas matrix-dominated transverse and shear properties may degrade above the glass-transition temperature of the matrix. The fatigue slope of the S-N curve also tends to become steeper at low temperature, so the same stress amplitude leads to fewer cycles to failure than at room temperature [11, 12].

2.4.2. Icing on wind turbine blades

In sub-zero conditions, supercooled water droplets that strike the blade freeze on contact and form layers of rime, glaze or mixed ice, mainly on the leading edge [6, 8]. Afzal and Virk [6] reviewed the operational, structural and economic consequences of icing on wind

turbines in cold regions and reported that ice accretion can reduce the annual energy production by 5 to 20 % and significantly increase the structural loads. Hu et al. [8] gave a more recent and comprehensive review of icing physics and de-icing technology, including the effect of ice on the airfoil shape, the center of gravity and the natural frequencies of the blade.

Numerical and experimental studies have quantified these effects. Bhatia and Al Wahaibi [29] simulated ice accretion on a typical airfoil and reported lift reductions up to 30 % and drag increases of more than 100 % for moderate icing conditions. Jin et al. [30] used a 2D and 3D CFD approach on a HAWT blade and showed that the ice mass per unit span is largest near the tip, where the relative wind speed and the collection efficiency are highest. Ozgen and Saribel [31] developed an improved roughness model that further increases the accuracy of icing predictions for airfoils. From a structural point of view, ice accretion adds mass without adding stiffness, which lowers the natural frequencies of the blade and may bring them closer to the rotor harmonics, so that resonance becomes a concern [8, 28].

2.4.3. Other environmental factors: hail, dust, lightning

Several other environmental effects are reported in the literature. Douvi et al. [22] studied the operation of a three-bladed HAWT under hailstorm conditions and showed that hail impacts modify the leading-edge geometry and reduce the lift-to-drag ratio. Douvi and Douvi [7] reviewed the broader category of "hazard environmental conditions" (icing, hail, sand, salt, lightning) and concluded that all of them shorten blade life by combining aerodynamic and structural effects. Sand and dust impacts are particularly relevant for inland sites such as Mongolia and the Gobi region, where dust storms progressively erode the gel coat and the outer plies of the laminate, increase surface roughness and reduce the energy yield. Long-term exposure to ultraviolet radiation, lightning strikes and freeze-thaw cycles further contribute to the degradation of the laminate [11, 18, 19].

2.5. Research gap and contribution of the present work

The literature reviewed above shows that the methodology of S-N-based fatigue analysis in commercial finite element codes is well established and that the favorable response of GFRP at low temperature has been demonstrated in several coupon-level experimental studies. However, blade-level fatigue simulations that explicitly use temperature-dependent S-N data extracted from OPTIMAT and that target the specific climate of Mongolia are still rare. Most published works either focus on aerodynamic effects of icing without modelling the structural fatigue [6, 29, 30], or perform isothermal

fatigue analyses without considering sub-zero conditions [13, 25, 26]. The present thesis contributes to closing this gap by combining a BEM-based load calculation, real wind data measured in Ulaanbaatar, and a fatigue analysis with three temperature-dependent S-N curves (room temperature, -40°C and +60°C) of GFRP. The result is a baseline that can be used and extended by future studies of wind turbine reliability in Mongolia.

3. Methodology

3.1. Model selection and wind data collection

Before the descriptions, one must know that selection of the models was not research of importance. The main reason to select is to have a reference parameter and design for the calculation of BEM and mechanical simulations, which are mandatory for this study.

3.1.1. Wind turbine design

BEM theory needs several geometric and operational quantities of the rotor, including the rotor radius, the number of blades and the rotor angular velocity [16, 17]. A specific commercial machine was therefore chosen to fix these inputs. Because the present work focuses on the behavior of a real wind turbine in cold conditions, a multi-megawatt class machine was preferred, since larger blades carry higher absolute loads and are more sensitive to fatigue [11]. The first wind farm built in Mongolia, commissioned in 2013 in Sergelen soum of Tüv province, about 75 km from Ulaanbaatar, is composed of 31 turbines of 1.6 MW each, installed by Clean Energy LLC. The corresponding model is the GE 1.6-100 (Fig.11), manufactured by GE Vernova, Inc. (Cambridge, Massachusetts). This machine was selected as the reference for the present study. The main specifications used in the calculations are listed in Table 1, and the complete datasheet is reproduced in Appendix.

Table 1. Necessary specifications of GE 1.6 - 100 wind turbine

GE Vernova 1.6 - 100	
Rated power, kW	1600
Cut-in wind speed, m/s	3.5
Rated wind speed, m/s	11
Cut-out wind speed, m/s	25
Rotor diameter, m	100
Number of blades	3
Max rotational speed, rpm	16.2
Tip speed, m/s	85
Material	GFRP
Hub height, m	80/100



Figure 11. GE 1.6-100 wind turbine

3.1.2. Airfoil

Several airfoil families have been proposed by different research agencies. One of them is the National Advisory Committee for Aeronautics (NACA), a United States federal agency founded in 1915 to support aeronautical research and dissolved in 1958, when its assets and personnel were transferred to NASA. During those years the committee produced a number of airfoil designs that are still in use today, among them the NACA 4412. The four digits encode the geometry: a maximum camber of 4 % of the chord, located at 40 % of the chord from the leading edge, and a maximum thickness of 12 % of the chord. This shape provides favorable aerodynamic performance at low to moderate Reynolds numbers and is therefore widely used in small-scale aerodynamic systems and in some wind turbine applications [31].

The airfoil shows a relatively high lift coefficient and a good lift-to-drag ratio, which leads to efficient energy conversion, as well as a smooth and predictable stall, which improves operational stability under varying flow conditions [17, 31]. Its moderate thickness offers a balance between aerodynamic efficiency and structural strength. Although more advanced airfoil families have been developed for modern large rotors, the NACA 4412 remains a reliable and well-documented choice for aerodynamic studies and simulations

[17]. The same shape is also used in light aircraft such as the Aeronca Chief series, in road vehicles for downforce or stability, and in small wind energy systems.

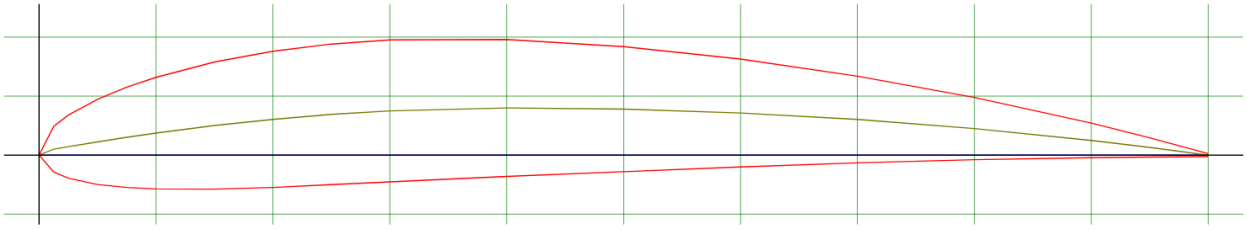


Figure 12. Cross section of NACA 4412 airfoil. Normally the coordinates are given, so that the geometry can be scaled.

3.1.3. Weather data

Even though generating wind data by an AI tool was possible, the use of real recorded wind data was encouraged to promote authenticity of the study. GMIT has a small weather station installed right next to the main building of the campus (Fig.13), which is a product of Hunan Rika Electronic Tech Co., Ltd, located in Changsha, China. The weather station had wind data recordings of summer, fall and spring. However, due to the freezing of components caused by severe weather conditions of Mongolian winter, some winter readings were missing. The recording contains data from October 1st, 2024 to April 1st, 2025 and a total of nearly 20000 lines of data. Selection of a range of data and processing was done in further steps.



Figure 13. Weather station at GMIT campus

3.2. Load calculation

3.2.1. Flapwise and edgewise bending moments

The two most important sectional loads on a wind turbine blade are the flapwise and edgewise bending moments. Both originate from the aerodynamic and gravitational forces described above, but they act in different directions and produce different stress patterns inside the blade [11, 16].

The flapwise direction is perpendicular to the rotor plane, that is the direction in which the blade bends “out of the plane” of rotation. The flapwise bending moment M_{flap} therefore mainly comes from the aerodynamic thrust. The edgewise direction is parallel to the chord of the airfoil and lies approximately in the plane of rotation. The edgewise bending moment Medge mainly comes from gravity and from the in-plane component of the aerodynamic force [16].

3.2.1.1. Calculation from BEM results

Once the normal and tangential forces per unit length, $p_n(r)$ and $p_t(r)$, are known from the BEM calculation, the bending moments at any radial station r_0 can be obtained by integrating the loads outboard of that station:

$$M_{flap}(r_0) = \int_{r_0}^{R} p_n(r)(r - r_0)dr$$

Equation 1. Flapwise bending moment

$$M_{edge}(r_0) = \int_{r_0}^{R} p_t(r) + p_g(r)(r - r_0)dr$$

Equation 2. Edgewise bending moment

where R is the rotor radius and $p_g(r)$ is the contribution of the blade weight per unit length, projected onto the edgewise direction. The largest values occur at the blade root, which is therefore the most critical cross-section for both static strength and fatigue [13, 16, 26].

3.2.1.2. Importance for fatigue

The flapwise moment is dominated by the steady mean thrust plus the fluctuating component caused by turbulence, wind shear and tower shadow. The edgewise moment is dominated by the once-per-revolution (1P) gravity reversal, plus aerodynamic in-plane forces and possible edgewise vibrations. Each rotor revolution therefore produces one fully reversed edgewise cycle and many smaller flapwise cycles. Over twenty years this corresponds to roughly 10^8–10^9 cycles per blade, which is why fatigue rather than static strength normally drives the design of the spar caps and the root region [11, 12, 13].

Spar caps are placed on the upper and lower surfaces of the airfoil to resist the flapwise moment, while reinforcement along the leading and trailing edges resists the edgewise moment. The combination of materials, geometry and ply orientation is optimized so that the laminate stays below its allowable fatigue stress in both directions during the design life [11, 13].

3.2.2. Blade element momentum (BEM) theory

The aerodynamic loads needed for fatigue analysis are most often computed by Blade Element Momentum theory. BEM combines two classical approaches: one-dimensional momentum theory applied to an annular streamtube and two-dimensional airfoil theory applied to a small radial element of the blade [16, 17].

3.2.2.1. Momentum theory

The actuator-disc model treats the rotor as an infinitely thin permeable disc. Applying conservation of mass, axial momentum and angular momentum to a streamtube of radius r and width dr gives the elementary axial thrust dT and torque dQ:

$$dT = 4\pi r \rho {V_0}^2 a(1-a)dr$$

Equation 3. Axial Thrust on the wind turbine

$$dQ = 4\pi r^3 \rho V_0 \Omega a'(1-a)dr$$

Equation 4. Resulting torque on the wind turbine shaft

where ρ is the air density, V_0 is the free-stream wind speed, Ω is the rotor angular velocity, a is the axial induction factor and a' is the tangential induction factor. The maximum theoretical efficiency of an ideal rotor is the Betz limit, equal to $16/27 \approx 0.593$ [16, 17].

3.2.2.2. Blade element theory

Blade element theory examines the forces on a small spanwise element of the blade. The relative wind speed seen by the element is

$$W = \sqrt{V_0{}^2(1-a)^2 + (\Omega r)^2(1+a')^2}$$

Equation 5. Relative wind speed

and the local angle of attack is $\alpha = \varphi - \theta$, where $\varphi = \tan^{-1}\frac{V^0(1-a)}{\Omega r(1+a')}$ is the inflow angle and θ is the local pitch plus twist. Lift and drag forces per unit span are then

$$dL = \frac{1}{2}\rho W^2 c C_L(\alpha) dr$$

Equation 6. Lift force applied on the airfoil

$$dD = \frac{1}{2}\rho W^2 c C_D(\alpha) dr$$

Equation 7. Drag force applied on the airfoil

where c is the local chord and CL, CD are the lift and drag coefficients of the airfoil section. These can be projected into the rotor plane to obtain the in-plane (tangential) and out-of-plane (normal) force components [16, 17].

3.2.2.3. Combined BEM equations

Equating the forces from blade element theory with the elementary thrust and torque from momentum theory gives the well-known BEM equations:

$$\frac{a}{1-a} = \frac{\sigma' C_n}{4F sin^2\varphi}$$

Equation 8. Equation for coefficient "a"

$$\frac{a'}{1+a'} = \frac{\sigma' C_t}{4F sin\varphi cos\varphi}$$

Equation 9. Equation for coefficient " a' "

where $\sigma' = \frac{Bc}{2\pi r}$ is the local solidity, B is the number of blades, $Cn = CLcos\varphi + CDsin\varphi$ and $Ct = CLsin\varphi - CDcos\varphi$ are the normal and tangential force coefficients, and F is the Prandtl tip- and root-loss correction. These equations are solved iteratively for a and a' at each radial station [16, 17].

3.2.2.4. Corrections and limitations

Several corrections are normally added to the basic BEM model to improve its accuracy. The Prandtl tip-loss factor F accounts for the finite number of blades; the Glauert correction replaces the simple momentum result for highly loaded rotors ($a > 0.4$); separate corrections are introduced for skewed inflow (yaw error) and for unsteady effects such as dynamic inflow and dynamic stall [16, 17]. Modern aero-elastic codes such as FAST, Bladed and QBlade implement BEM with all these corrections and couple it to a structural model of the rotor. Although BEM cannot capture three-dimensional flow effects in detail, comparisons with computational fluid dynamics show that, for normal operating conditions, BEM predicts the integrated rotor loads with an accuracy that is sufficient for design and fatigue analysis [17].

3.2.3. BEM theory calculation using Python

The raw data from the weather station contains very low wind speeds because of its installation location, which is on the ground and right next to the main building of GMIT campus. The data recorded in winter were extremely low and still, which led to the selection of more fluctuating wind speeds recordings. Recordings from 15th of October have shown higher readings and significant variation with maximum wind speed of 7.8 m/s, mean of 1.95 m/s, and standard deviation of 1.17. Additionally, the wind speed readings were raised by 8.9 to be distributed around the rated wind speed of the model, which will cause maximum loads on the blade.

The main target loads, flapwise and edgewise bending moments, can be extracted from the BEM calculation result. An AI tool called Claude by Anthropic PBC produced promising results by generating python code to calculate the loads. The following section demonstrates how the code was constructed.

3.2.3.1. Python code construction

The BEM analysis was implemented in Python, structured sequentially across six logical stages. The code begins by defining all turbine parameters sourced directly from the GE Vernova GE 1.6-100 datasheet, including a rotor radius of 50 m, rated power of 1,600 kW, cut-in and cut-out wind speeds of 3.5 m/s and 25 m/s respectively, and a maximum rotor speed of 16.2 RPM. These constants serve as the foundation for all subsequent calculations.

The CAD model collected from the GrabCAD community did not specify the chord and twist distributions of the blade. Therefore, the blade geometry was constructed using the Betz-optimal (Schmitz) approach, where the blade span was discretized into 30 radial elements between the hub and tip [16, 17]. For each element, the optimal chord length and twist angle were derived analytically as a function of the local tip speed ratio, the design angle of attack of 5°, and the corresponding lift coefficient of NACA 4412 at that angle ($Cl = 1.025$ at $Re = 1{,}000{,}000$).

The aerodynamic polar data for the NACA 4412 airfoil was obtained from Xfoil at a Reynolds number of 1,000,000, covering an angle of attack range of −15.75° to 18.75°. Since the BEM solver requires lift and drag coefficients across the full 360° range to handle post-stall and parked conditions, the polar was extended to ±180° using the Viterna-Corrigan extrapolation method [17]. The resulting Cl and Cd curves were stored as interpolation functions for efficient lookup during the iterative solve.

The core of the implementation is the BEM solver, which operates element by element along the blade span. For each element, the axial and tangential induction factors were solved iteratively until convergence within a tolerance of 1×10^{-7}, with under-relaxation applied at 50% to ensure numerical stability. Prandtl tip-loss and hub-loss corrections were applied multiplicatively at each iteration, and the Buhl–Glauert correction was activated for heavily loaded conditions where the axial induction factor exceeded 0.4 [16, 17]. Upon convergence, the normal and tangential force components were integrated spanwise to obtain rotor thrust, torque, shaft power, and per-blade flapwise and edgewise root bending moments.

A control logic layer was implemented to replicate realistic turbine operation across the full wind speed range. Below rated wind speed, the rotor speed was varied to maintain the design tip speed ratio at zero collective pitch. Above rated wind speed, the rotor speed was fixed at 16.2 RPM, and a bisection algorithm was used to find the collective

pitch angle that regulated output power to exactly 1,600 kW [16]. For wind speeds exceeding the cut-out threshold of 25 m/s, the blades were set to a feathered position of 89° with the rotor at rest, representing the parked survival state.

Finally, the solver was executed across all 183 wind speed entries from the input time-series dataset from 15th October readings. The results, including pitch angle, rotor speed, power, thrust, torque, and both bending moment components, were exported to a CSV file and visualized as scatter plots against wind speed, color-coded by operating mode. A secondary smooth power and load curve was also generated by sweeping wind speed from 0 to 30 m/s at 0.5 m/s intervals. The whole result is shown as a table in the Appendix.

3.3. Numerical Analysis

3.3.1. General features of ANSYS Mechanical

ANSYS Mechanical is a comprehensive finite element analysis (FEA) software developed by ANSYS, Inc. that is widely used in engineering and research for simulating the structural and mechanical behavior of components and assemblies, which is the reason why it was chosen. ANSYS Mechanical provides a powerful simulation environment that enables engineers and researchers to predict how structures respond to various physical loads, including forces, pressures, thermal conditions, and vibrations. It is built upon the FEM, a numerical technique that discretizes complex geometries into smaller elements to solve governing equations of mechanics across the entire domain. The key capabilities of the software include:

- Static Structural Analysis – Evaluates stress, strain, and deformation under static loading conditions.
- Modal Analysis – Determines the natural frequencies and mode shapes of a structure.
- Transient Dynamic Analysis – Examines time-dependent structural responses under varying loads.
- Thermal Analysis – Assesses heat transfer and temperature distribution within components.
- Fatigue Analysis – Predicts component life under cyclic loading.

- Nonlinear Analysis – Handles geometric nonlinearity, material plasticity, and contact mechanics.

ANSYS Mechanical integrates perfectly with ANSYS Workbench, a unified simulation platform that supports multi-physics coupling and parametric studies. It supports a wide range of material models and is compatible with CAD platforms such as SolidWorks, CATIA, and AutoCAD. Due to its versatility and accuracy, ANSYS Mechanical is extensively used in academic research, as it has appeared in numerous scientific papers, as well as in industries such as aerospace, automotive, civil engineering, and biomedical engineering.

3.3.2. Concept of fatigue and the S-N curve

3.3.2.1. Definition of fatigue

Fatigue is the gradual weakening and final fracture of a material that is subjected to many cycles of fluctuating stress, even when the maximum stress is well below the static strength [12]. Three stages are usually identified: crack initiation, stable crack growth and final fast fracture. For metals, the boundary between high-cycle and low-cycle fatigue is conventionally placed near 10^4–10^5 cycles. Wind turbine blades typically experience between 10^8 and 10^9 cycles during a 20-year life and therefore lie almost entirely in the high-cycle regime [11, 12].

3.3.2.2. Stress cycle parameters

A general fluctuating stress cycle is described by the maximum stress σ_{max}, the minimum stress σ_{min}, the mean stress $\sigma_m = \frac{(\sigma_{max} + \sigma_{min})}{2}$, the stress amplitude $\sigma_a = \frac{(\sigma_{max} - \sigma_{min})}{2}$ and the stress ratio $R = \frac{\sigma_{min}}{\sigma_{max}}$. The case $R = -1$ corresponds to fully reversed loading, $R = 0$ to a tension–zero cycle and $0 < R < 1$ to tension–tension loading. Each value of R produces a different fatigue curve, which is the reason why composite databases store separate S-N data for several R-values [12, 14].

3.3.2.3. The S-N curve

The Wöhler diagram, or S-N curve, plots the stress amplitude S (or stress range $\Delta\sigma$) against the number of cycles to failure N on a logarithmic scale. For many steels the curve becomes horizontal beyond about 10^6 cycles, defining a fatigue limit below which the material has practically infinite life. For aluminum alloys and composites the curve continues to decrease, and no clear endurance limit is observed [21].

In the high-cycle regime the S-N curve is often described by Basquin's relation:

$$\sigma a = \sigma_f'(2N_f)^{\mathrm{b}}$$

Equation 10. Basquin relation

or, equivalently, by the simple power law

$$S = A \cdot N^{-\frac{1}{m}}$$

Equation 11. Relation including the slope of the S-N curve "k"

where A and m (sometimes written as the slope $k = \frac{1}{m}$) are material constants determined by fitting test data. For glass-fiber reinforced polymers (GFRP) the slope m is typically between 9 and 12, while for carbon-fiber composites it is between 14 and 20, meaning that carbon laminates are less sensitive to load amplitude [11, 12].

3.3.2.4. Fatigue of composite materials

Composite blades are made mostly of GFRP and increasingly of CFRP for the spar caps. Fatigue in composites is fundamentally different from fatigue in metals because damage does not propagate from a single dominant crack but accumulates as a distributed network of matrix micro-cracks, fiber–matrix debonding, delamination and finally fiber breakage [11, 12, 23]. The progression of stiffness loss is therefore commonly used as an indicator of damage. Colombo et al. [23] presented detailed measurements of stiffness reduction during fatigue tests of GFRP coupons and showed that the residual stiffness can be modelled as a smooth function of the cycle ratio n/N.

Two large research programmes provide the experimental basis for most fatigue analyses of blade composites: the European OPTIMAT BLADES project [14] and the SNL/MSU/DOE Composite Material Fatigue Database [27]. Both produced extensive S-N data for unidirectional and multidirectional laminates at several R-values, meaning stresses and temperatures. The PhD thesis of Nijssen [12] is one of the most cited works in this field and provides constant-life diagrams that allow the engineer to convert tests at one R-value into design curves for any other R-value.

3.3.2.5. Damage accumulation

For variable-amplitude loading, the most widely used rule is the linear cumulative damage law of Palmgren and Miner [21]:

$$D = \sum_{i=1}^{n} \frac{n_{\mathrm{i}}}{N_{\mathrm{i}}}$$

Equation 12. Miner's rule

where n_i is the number of cycles applied at stress level i and N_i is the number of cycles to failure at the same level taken from the S-N curve. Failure is predicted when D reaches one. Although Miner's rule is known to be approximate, it is used in design standards such as IEC 61400-1 and Germanischer Lloyd because of its simplicity. The variable load history is usually decomposed into discrete cycles by the rainflow counting method. Kong et al. [13] applied the linear damage rule together with the load spectrum and Spera's empirical equations to estimate the fatigue life of a 750 kW HAWT blade and demonstrated that the method is suitable for industrial design when reliable S-N data are available.

Shokrieh and Rafiee [26] later proposed a more advanced approach in which the material properties of every laminate ply are gradually degraded according to the local stress, and the analysis is repeated until failure. Their stochastic finite-element simulation of a full composite blade reproduced realistic fatigue failures at the spar cap and root and confirmed that the linear damage rule overestimates the life of strongly stressed regions.

3.3.3. Simulation setup

GFRP was selected as the material for the model and the fatigue life was added manually to its engineering data on ANSYS Workbench as it was missing in the first place. The added data was extracted from the OptiDAT database of the OPTIMAT BLADES project operated from 2002 to 2006 in Europe. However, the database itself was not directly available due to the unresponsive link to it. Therefore, an example graph shown on Fig. 14 was found and values were extracted by digitizing the graph. The material data was duplicated 2 times because of the S-N curve at three different temperatures, room temperature, -40°C and 60°C. This finding created a crucial baseline for this study.

The model was collected from the GrabCAD community, an internet website containing numerous free-to-use CAD models. To align with the GE 1.6-100 model specifications mentioned above, the CAD model was scaled up to match the rotor radius of 50 meters. The final model was imported into ANSYS Workbench as a geometry.

Both fatigue and vibration analysis can be done in ANSYS Mechanical. To conduct fatigue analysis, it is mandatory to run static structural analysis on the model, which

creates the baseline for the fatigue analysis. The fixed support was set at the root and the flapwise and edgewise bending moments were added on the blade separately. The application is shown on Fig.15. Then the fatigue tool was inserted in the solution part and the previously calculated bending moments on the blade were imported into the fatigue tool as a load history data.

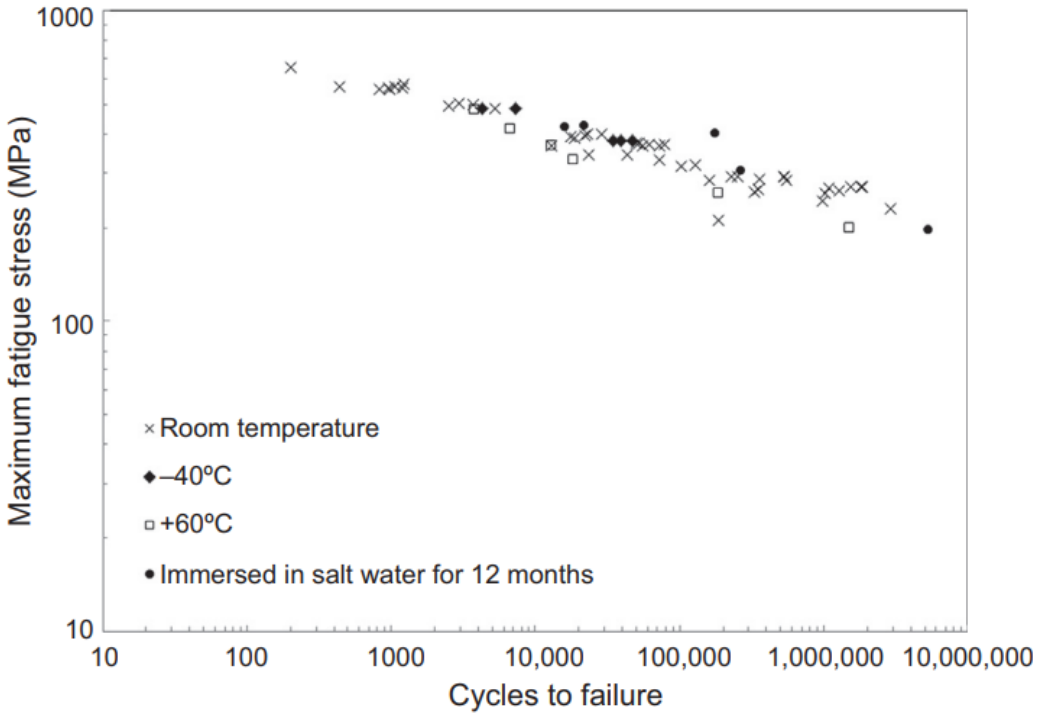


Figure 14. S-N curve of GFRP at different environmental conditions extracted from OptiDAT database [15]

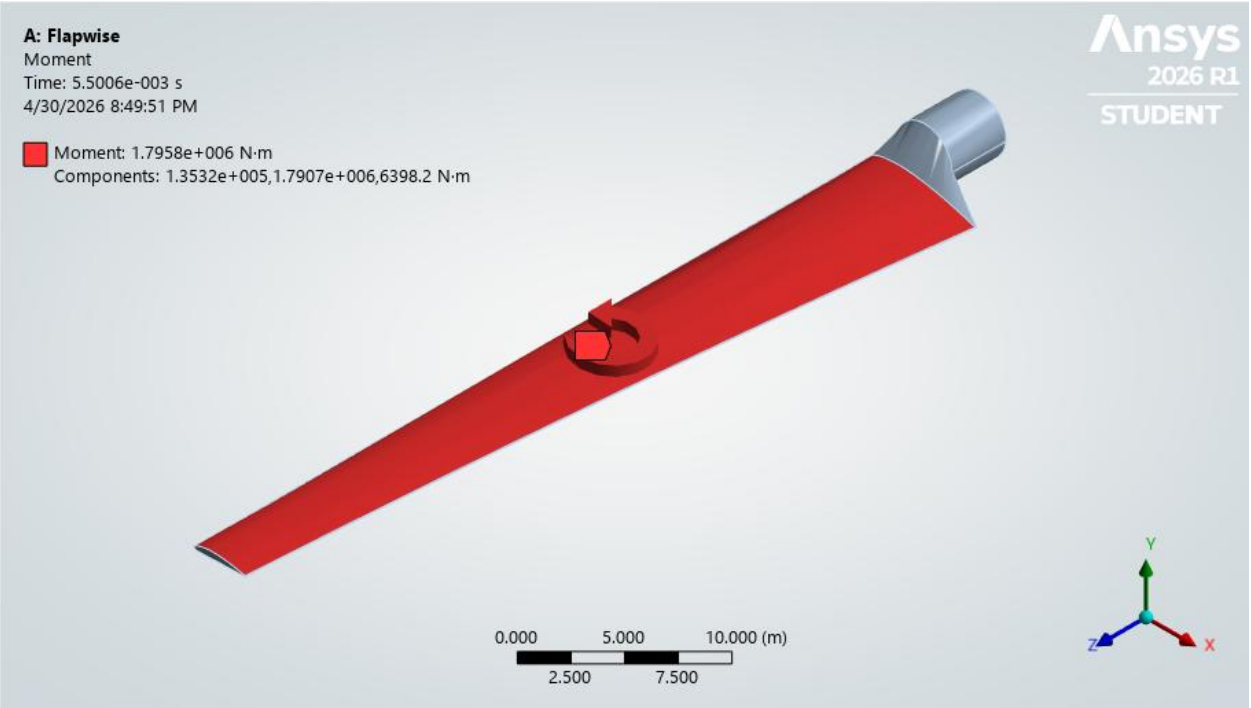


Figure 15. Model installed from GrabCAD community repository and loading direction

3.3.4. Fast Fourier Transform of the wind speed signal

The frequency content of the wind speed signal is needed for the resonance assessment of the blade. The Fast Fourier Transform (FFT) of a discrete signal x[n] of length N is defined as

$$X[k] = \sum_{n=0}^{N-1} x[n] \cdot e^{-\frac{j2\pi kn}{N}}$$

$$k = 0, 1, \dots, N-1$$

Equation 13.Fast Fourier Transform of X[n] discrete signal

The FFT was computed in Google Sheets with the free "XLMiner Analysis Toolpak" add-on. The signal was first centered by subtracting its meaning and then multiplied by a Hanning window

$$w[n] = 0.5 \cdot \left(1 - \cos\left(\frac{2\pi n}{N-1}\right)\right)$$

$$n = 0, 1, \dots, N-1$$

Equation 14. Hanning window

which suppresses spectral leakage from the finite-length truncation. Only the first N/2 + 1 coefficients are physically meaningful because the input is real-valued, so the spectrum is symmetric about k = N/2. The magnitude and the corresponding physical frequency of bin k are

$$|X[k]| = \sqrt{Re(X[k])^2 + Im(X[k])^2}$$

Equation 15. Magnitude of the resulting complex number

$$f_{\mathrm{k}} = k \cdot \frac{f_s}{N}$$

Equation 16. Corresponding frequency

where f_s is the sampling frequency. The Nyquist frequency $f_{\mathrm{n}} = \frac{f_s}{2}$ is the highest frequency that can be represented without aliasing.

3.4. Analysis assumptions

The aim of the assumptions was to streamline the modelling and simulation process for several reasons, such as implementing existing trends for parameters that are unknown, simplification, consideration of extreme conditions, and assuming parameters that are beyond scope of the study. Due to these reasons, number assumptions were made.

As mentioned before, the readings of the weather station were very low due to the installation location. Therefore, the wind speed readings were raised by 8.9 m/s, which was considered by subtracting the rated wind speed of the chosen wind turbine model by the mean of the real reading. According to the pitch control system of the wind turbine blade, the power generation will reach its peak starting from 11 m/s and the wind load on the blade will be at its highest, which is a favorable number for fatigue analysis.

Deep study of blade aerodynamics and its shape parameters is beyond the scope of this study. Therefore, selection of existing CAD models was encouraged. The coordinates and polar data containing list and drag coefficients at the corresponding angle of attack was provided by the sources online. However, the chord and twist distributions of the blade were not provided, which are an important parameter when it comes to using BEM theory for calculation. Implementation of the Betz-optimal approach tackled this problem as mentioned before.

A typical S-N curve, otherwise known as Wöhler diagram, is a way of showing the mechanical component's fatigue characteristics at varying stress amplitudes, where the

line is the representation of the component's failure chance of 50 percent at the corresponding stress amplitude. Without this line, the chart will look like numerous data points scattered across certain regions of the chart. The digitized values, shown on Fig.16 were then represented by a logarithmic equation using Google sheets, which then imported into the material data on ANSYS Workbench.

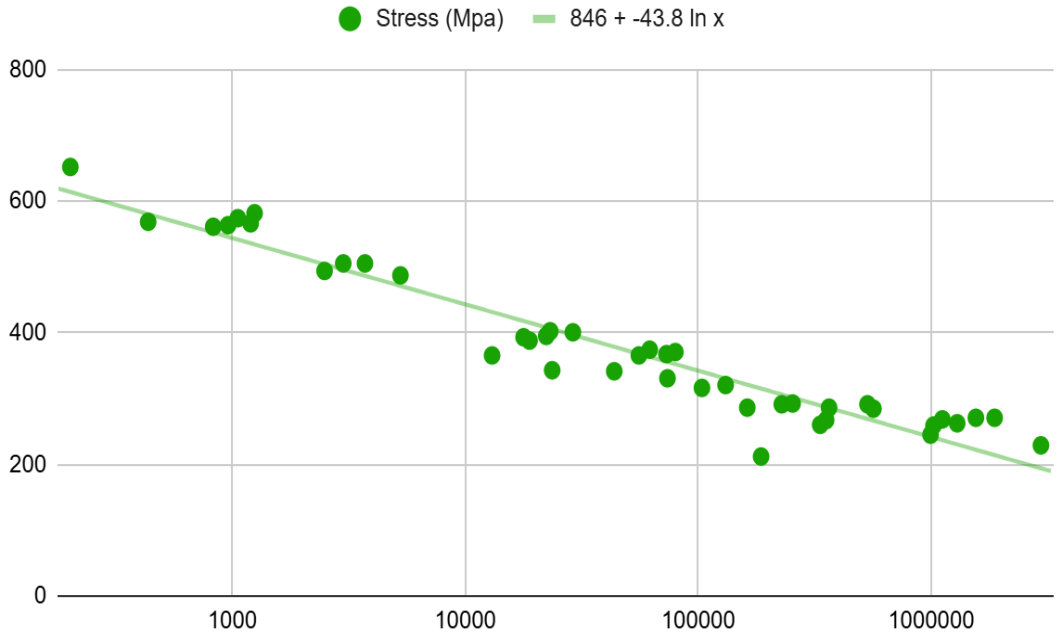


Figure 16. S-N curve of GFRP at room temperature and its trendline [15]

ANSYS Workbench has a material database in its engineering data and GFRP can be found as "PCB laminate, Epoxy/Glass fiber, FR-4.0 (Df > 0.02 at 10GHz)" in ANSYS GRANTA folder. The material has its mechanical properties, namely density, isotropic secant coefficient of thermal expansion, isotropic elasticity, tensile yield and ultimate strength. However, these properties are not readily available in different environmental conditions. Therefore, the only varying property was fatigue life. Other properties were assumed to be the same at varying temperatures.

In resonance risk assessment, the lowest natural frequency of the blade was 0.273 Hz and the comparison with the real load history in frequency domain was not possible with Δt of 60 seconds, giving the maximum sampling frequency of 0.0167 Hz. To match with the natural frequency, the sampling frequency was assumed to be 10 Hz, which means Δt of 0.1 seconds. This range enables the possibility to check 4 modes of natural frequency.

4. Results and discussion

4.1. Selection of the element size

The most important step before the structural simulations is the choice of an appropriate element size for the mesh. Mesh independence was investigated by checking the convergence of the results. Several test runs with different element sizes were carried out under a flapwise bending moment of 500 MNm and a zero-based fatigue loading. A uniform element sizing was used to avoid the appearance of outliers caused by local mesh refinement.

Table 2 shows that apparent convergence is reached for element sizes between 2 m and 0.875 m: the equivalent stress, the equivalent elastic strain and the predicted fatigue life deviate from their respective means by only 0.64 %, 0.84 % and 3.74 %. However, an inspection of the element quality histogram, which is generated by setting the mesh metric in ANSYS Mechanical to "Element Quality", gives a different picture. The metric varies between 0 and 1, with 1 corresponding to a perfectly shaped element. As shown in Fig.17, the mesh produced with an element size of 1 m, and in fact every size between 2 m and 0.875 m, contains a significant number of strongly degenerative elements. The apparent numerical convergence is therefore misleading, and the smaller sizes had to be re-examined.

Table 2. Static and fatigue results obtained at different element sizes

Element size, m	Elements	Nodes	Eq. stress max, MPa	Eq. stress min, MPa	Eq. elastic strain max	Eq. elastic strain min	Life, cycles
2	505	1153	2.6173e+08	4.6743e+05	1.086e-02	2.3284e-05	6.2123e+05
1.75	770	1633	2.5911e+08	3.111e+05	1.070e-02	1.5045e-05	6.5951e+05
1.5	967	2048	2.5792e+08	2.9786e+05	1.062e-02	1.4361e-05	6.7763e+05
1.375	1085	2317	2.5926e+08	3.5912e+05	1.0643e-02	1.7657e-05	6.5729e+05
1.25	1219	2616	2.597e+08	4.116e+05	1.0676e-02	4.5094e-05	6.5074e+05

1.125	1553	3289	2.5716e+08	2.8131e+05	1.058e-02	2.0484e-05	6.8953e+05
1	1973	4130	2.5673e+08	3.0242e+05	1.0732e-02	1.7528e-05	6.9638e+05
0.875	2680	5463	2.5737e+08	2.154e+05	1.077e-02	1.1873e-05	6.8621e+05
0.75	3874	7644	2.8821e+08	1.6917e+05	1.2304e-02	1.0187e-05	3.3935e+05
0.625	6351	11921	2.9854e+08	2.1388e+05	1.2844e-02	1.0092e-05	2.681e+05
0.5	12102	21474	2.867e+08	1.4112e+05	1.2677e-02	9.0578e-06	3.5132e+05
0.375	27274	45412	3.0515e+08	1.176e+05	1.317e-02	6.1315e-06	2.3053e+05
0.3	53753	85991	3.1098e+08	46180	1.3623e-02	2.9175e-06	2.0181e+05

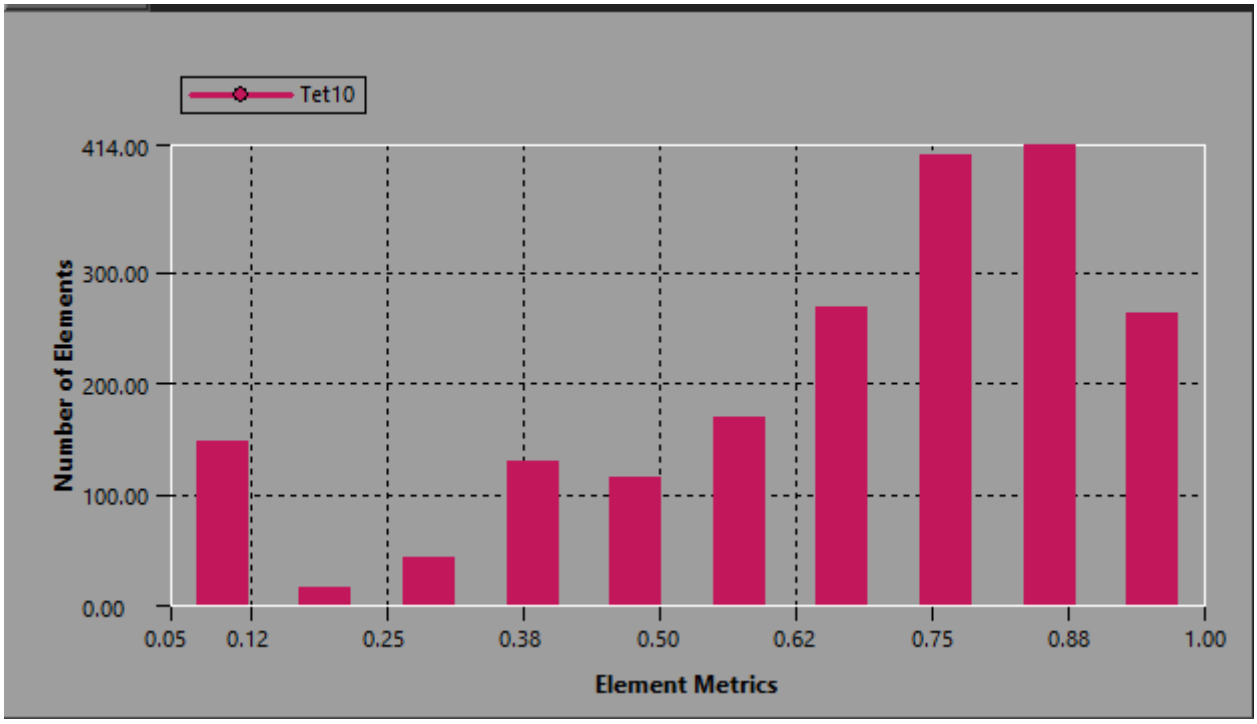


Figure 17. Element-quality histogram for an element size of 1 m

Once the meshes were regenerated, the smaller element sizes show a much smaller share of degenerated elements. The selection of the final mesh size, however, must still be made carefully because the relative scatter of the results changes substantially at small sizes: the equivalent stress, the equivalent elastic strain and the predicted fatigue life vary by 3.53 %, 3.87 % and 23.6 %, respectively (Table 3). The element-quality

statistics show that the size of 0.375 m gives the highest average element-quality metric, the lowest standard deviation and the smallest fraction of degenerated elements as shown in Fig.18. This element size was therefore retained for all subsequent simulations.

Table 3. Element-quality statistics at the smaller mesh sizes

Element size, m	Min	Max	Average	Standard deviation
0.75	0.066284	0.99991	0.73471	0.21074
0.625	0.080319	0.99975	0.75329	0.18605
0.5	0.10985	0.99997	0.78432	0.15422
0.375	0.17102	0.99996	0.80544	0.12942
0.3	0.048711	1	0.80095	0.15031

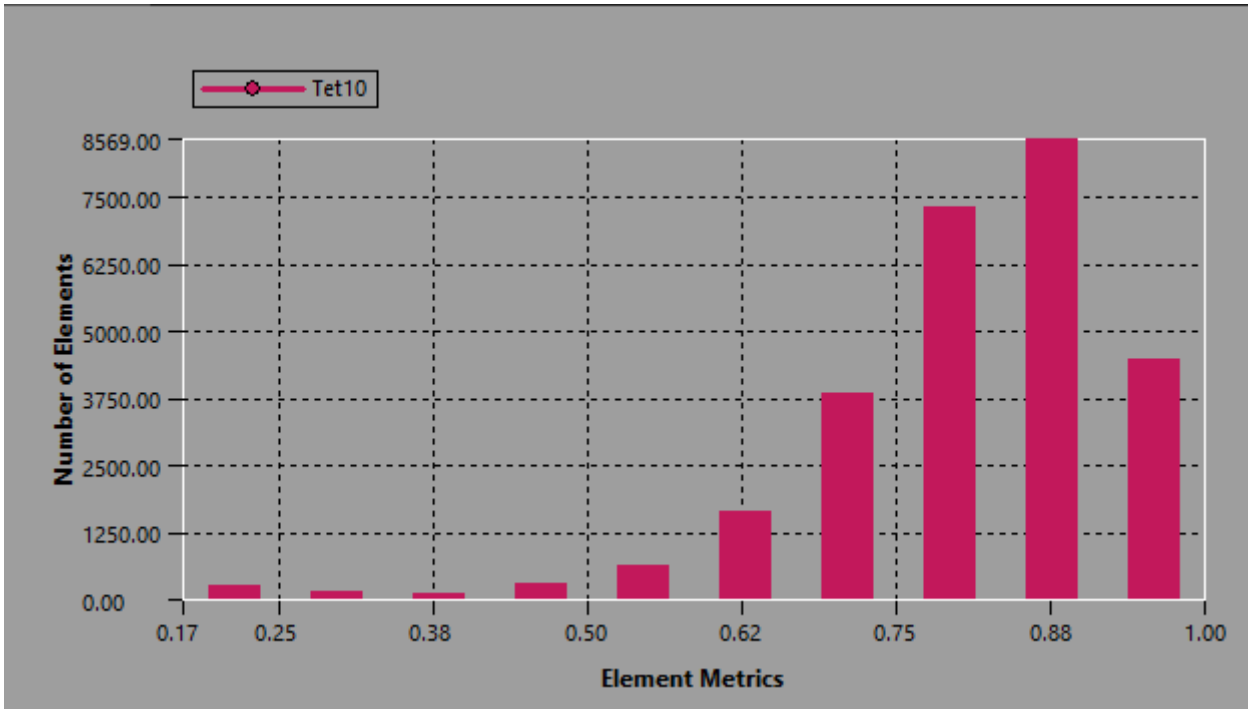


Figure 18. Element-quality histogram for an element size of 0.375 m

The need for a careful mesh study before any fatigue calculation is consistent with similar finite-element investigations of composite blades. Tawade et al. [25] performed a parametric ANSYS study of a GFRP blade and reported that the predicted fatigue life is highly sensitive to the local refinement at the root, where the bending stresses concentrate. Navadeh et al. [28] arrived at the same conclusion in their modal analysis of a HAWT blade in ABAQUS, where a coarse mesh shifted the natural frequencies by several percent. The behavior observed in Table 2, in which a numerical convergence in stress and life is accompanied by a poor element-quality distribution, confirms that pure value-based convergence is not sufficient and must be combined with a quality check, as also recommended in the ANSYS theory documentation.

4.2. Fatigue analysis

The static structural analysis returns the von Mises equivalent stress, the equivalent elastic strain and the deformation field. Adding the fatigue tool to the solution branch produces the additional outputs:

- Life;
- Damage;
- Safety factor;
- Biaxiality indication;
- Fatigue sensitivity.

The maximum flapwise and edgewise bending moments obtained from the BEM calculation were 1795.812 kNm and 294.116 kNm, respectively, and were applied as moments at the blade root. The load ratio was set to $R = 0$, because the load history obtained from the BEM solver contains only positive (tensile) values. The result shown in Fig.19a and 19b indicates that the blade can sustain more than one hundred million cycles at both maximum flapwise and edgewise bending moments, that is, the maximum flapwise loading does not break the blade. The other fatigue outputs confirm this conclusion: no damage is computed, and the safety factor is everywhere larger than 15.

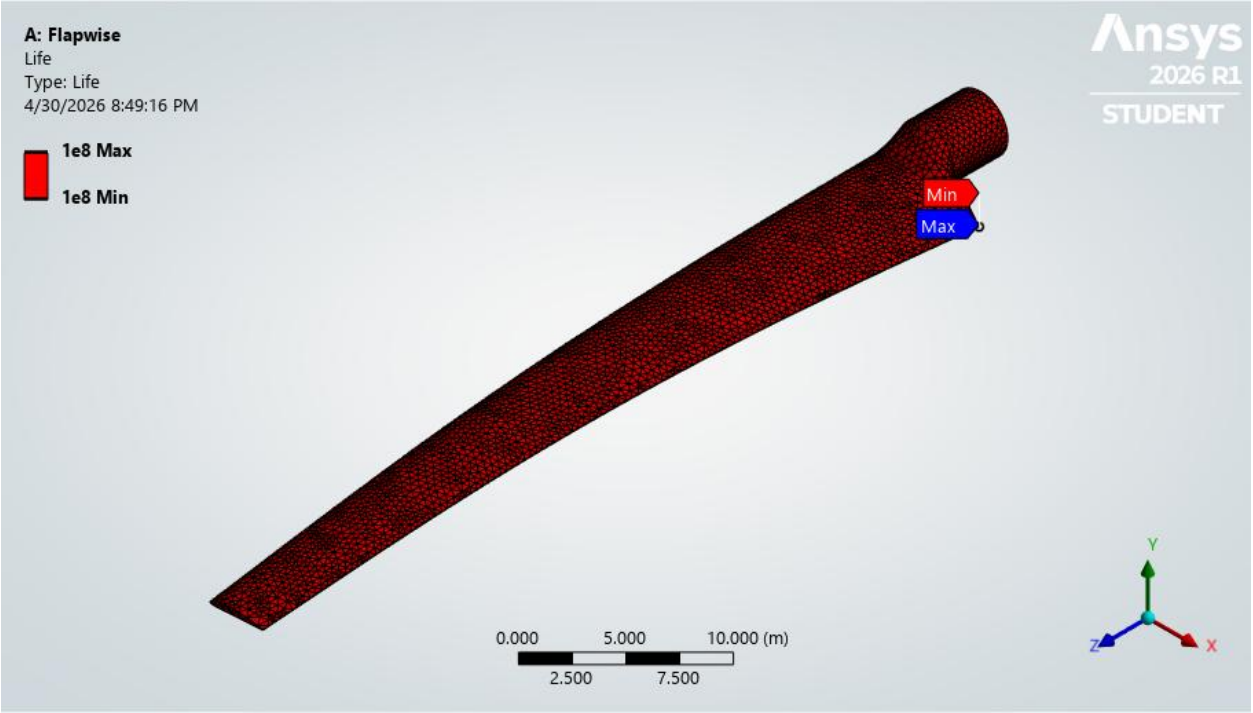


Figure 19a. Fatigue analysis result for a zero-based maximum flapwise bending moment

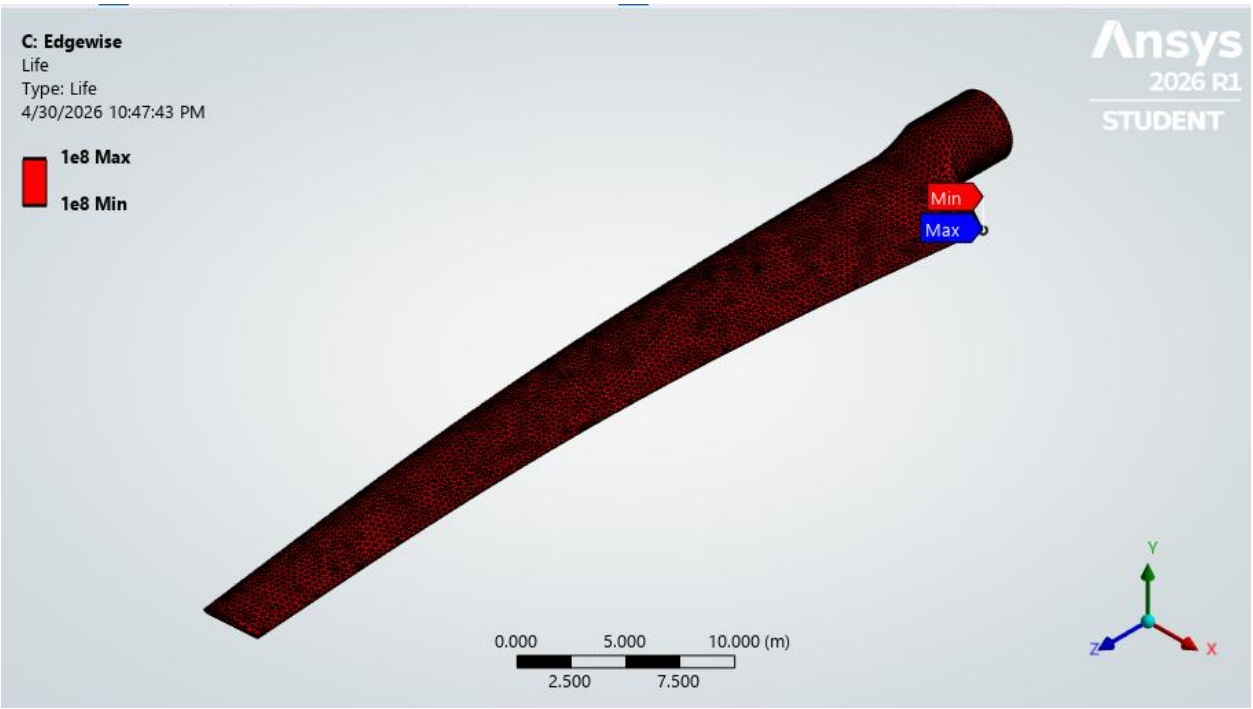


Figure 19b. Fatigue analysis result for a zero-based maximum edgewise bending moment

A similar conclusion is reached when the full operational loading is applied, as shown in Fig.20a, 20b, 21a, and 21b. The unit of life is now "blocks", where each block corresponds to one full repetition of the load spectrum, instead of cycles. The result indicates that the spectrum can be repeated 17.857 and 17.544 million times before failure occurs.

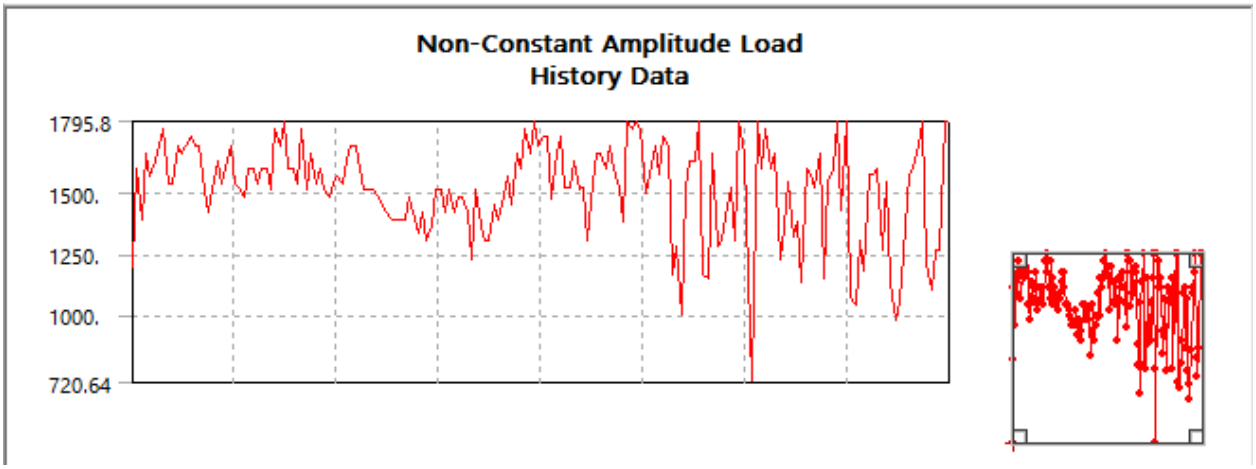


Figure 20a. Flapwise bending load history

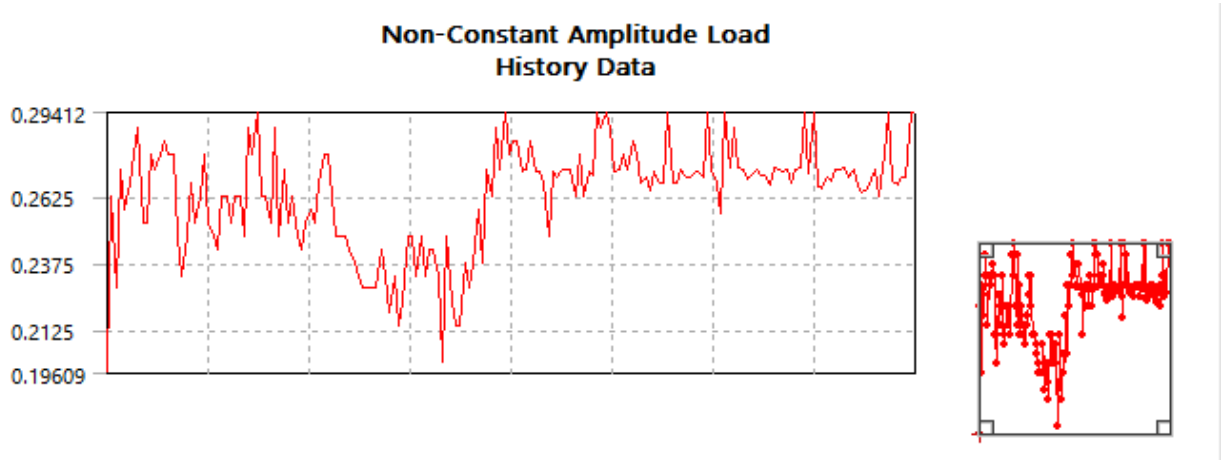


Figure 20b. Edgewise bending load history

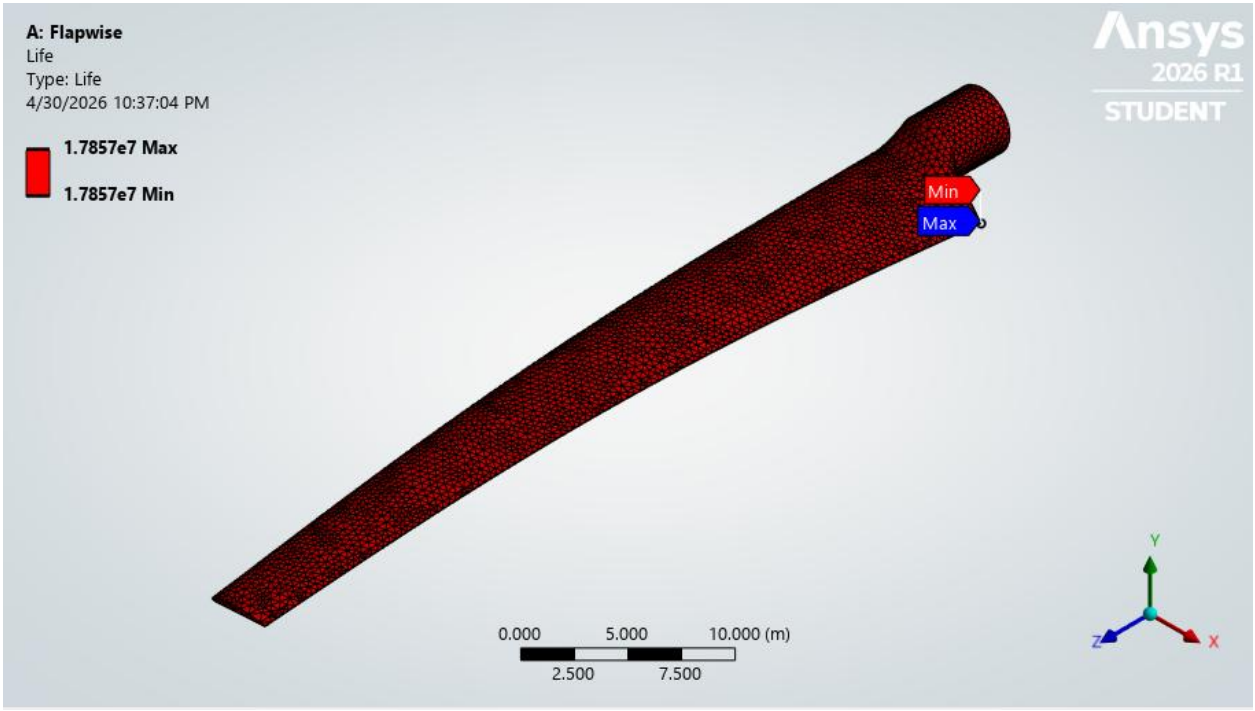


Figure 21a. Fatigue result under flapwise operational loading

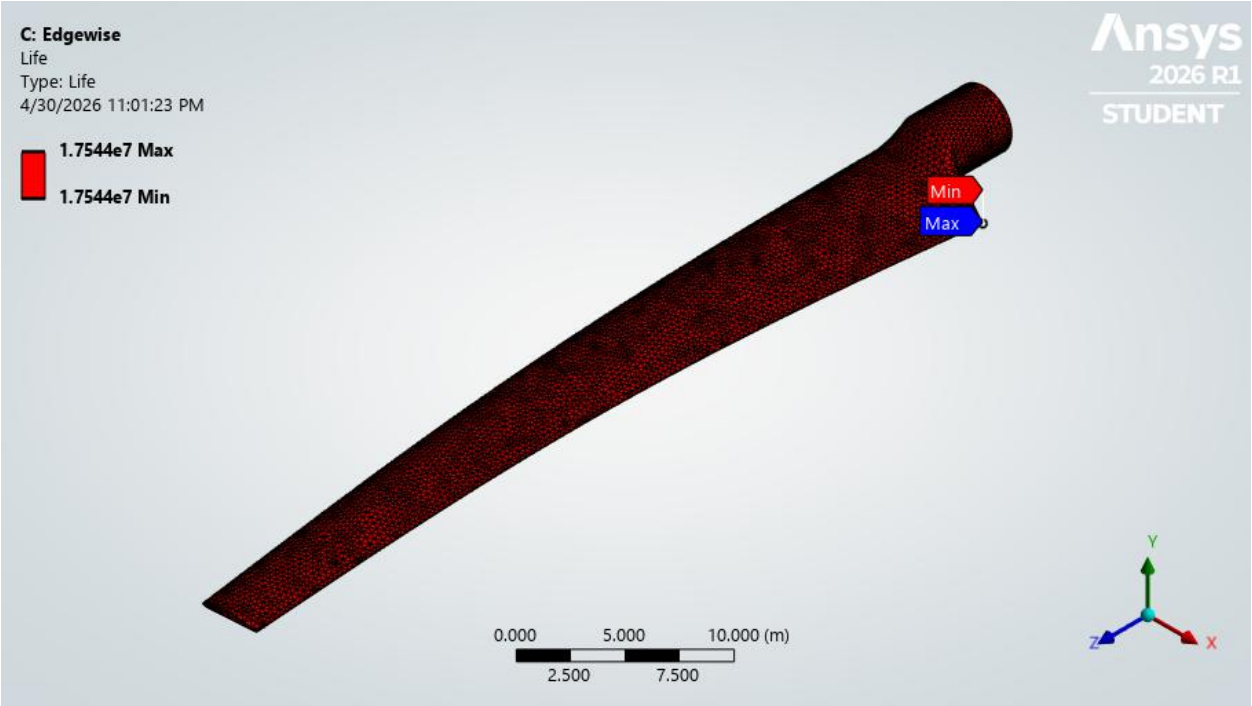


Figure 21b. Fatigue result under edgewise operational loading

The very large safety factor obtained at room temperature (greater than 15) is in line with the design philosophy of modern blades, which keeps the spar caps and the root region well below the fatigue limit of GFRP during normal operation [11, 12]. Kong et al. [13] applied the linear S-N damage rule together with the load spectrum and Spera's empirical formulae to a 750 kW blade and predicted a fatigue life longer than the 20-year design target, which is qualitatively similar to the result of the present work. Shokrieh and Rafiee [26], on the contrary, used a stochastic finite-element model with progressive material degradation and reported failures at the spar cap and at the root after a few million blocks for a similar blade. The difference between the two approaches highlights a known limitation of the linear damage rule used in ANSYS, which tends to overestimate the fatigue life of composites [12, 23]. The high safety factor reported here must therefore be interpreted as an upper bound and because of the simplifications adopted in the geometry and in the damage rule, and not as evidence that the blade has unlimited margin. Chou et al. [20] showed in their analysis of a real blade failure under typhoon loading that catastrophic root failures occur at moments comparable to those simulated here, which underlines the importance of also studying extreme load cases beyond the operating spectrum.

4.2.1. Fatigue results at different temperatures

To highlight the influence of the environmental conditions, both flapwise and edgewise bending moment was then ramped up from 1 MNm to 500 MNm and 100 MNm. Before

running the simulations and finding the OptiDAT database, the working hypothesis was that GFRP would behave better at lower temperatures and worse at higher temperatures, in line with the experimental observations of Jia et al. [10] for CFRP in three-point bending between -100°C and 100°C. The same trend was reported for unidirectional GFRP between -25°C and 100°C by Ou et al. [9], who measured an increase of tensile strength and modulus and a reduction of the failure strain when the temperature was lowered. The simulation results obtained with the OptiDAT data confirm the hypothesis. Figures 22a, 22b, 22c, 22d, 22e, and 22f show the fatigue contours produced by the ANSYS fatigue tool at room temperature, at -40°C and at +60°C. A clearly smaller fraction of the blade volume reaches the failure threshold at -40°C than at the higher temperatures, which suggests that low temperature alone is not a critical factor for the operation of the GFRP blade in Mongolian winters.

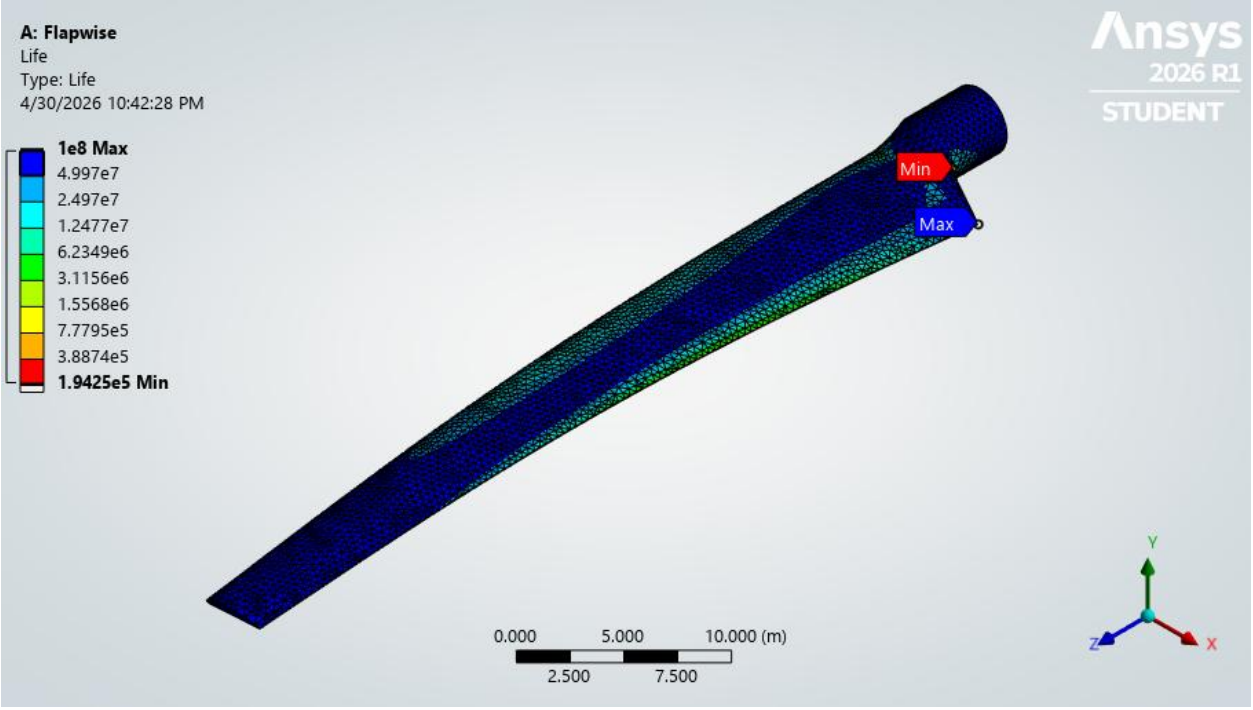


Figure 22a. Fatigue contour of zero-based flapwise bending of the GFRP blade at room temperature

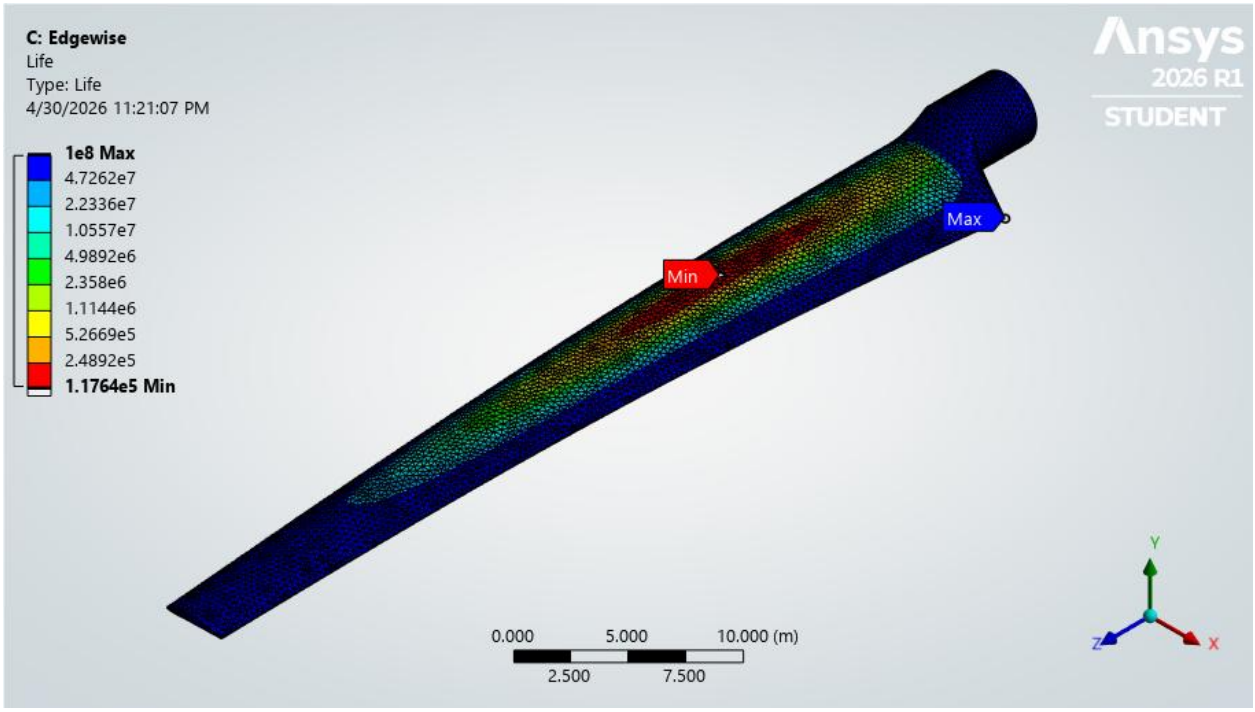


Figure 22b. Fatigue contour of zero-based edgewise bending of the GFRP blade at room temperature

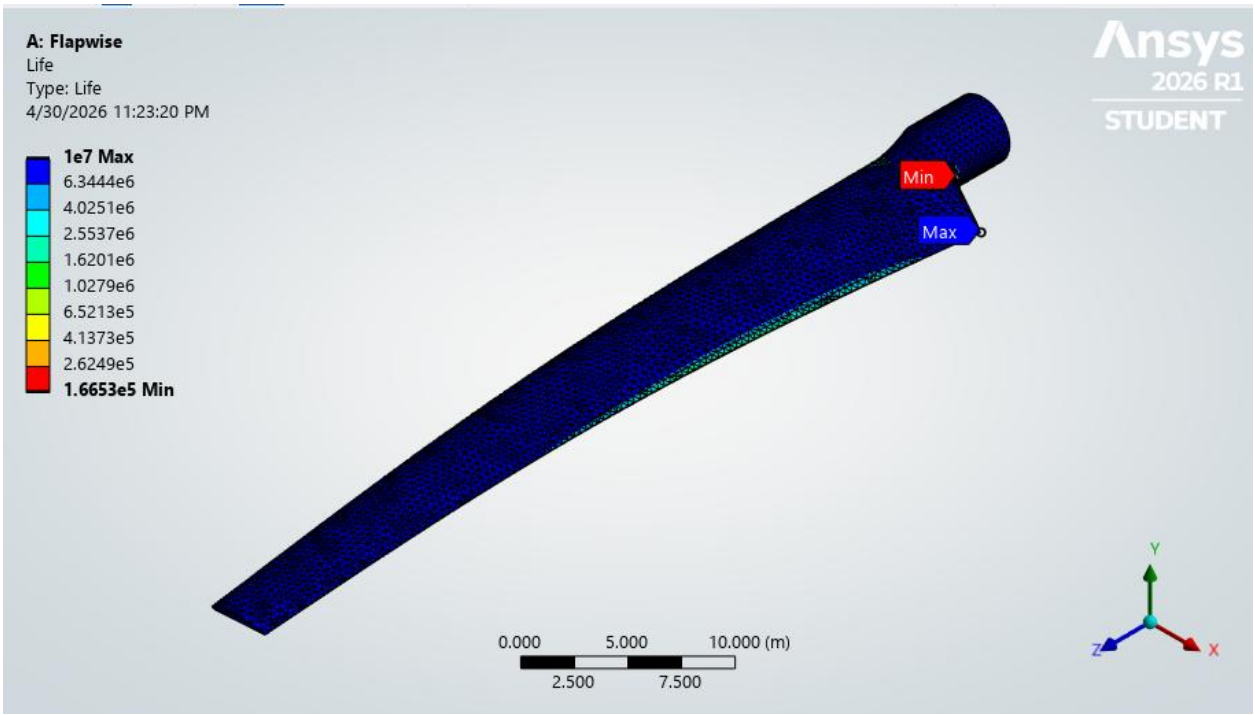


Figure 22c. Fatigue contour of zero-based flapwise bending of the GFRP blade at -40°C

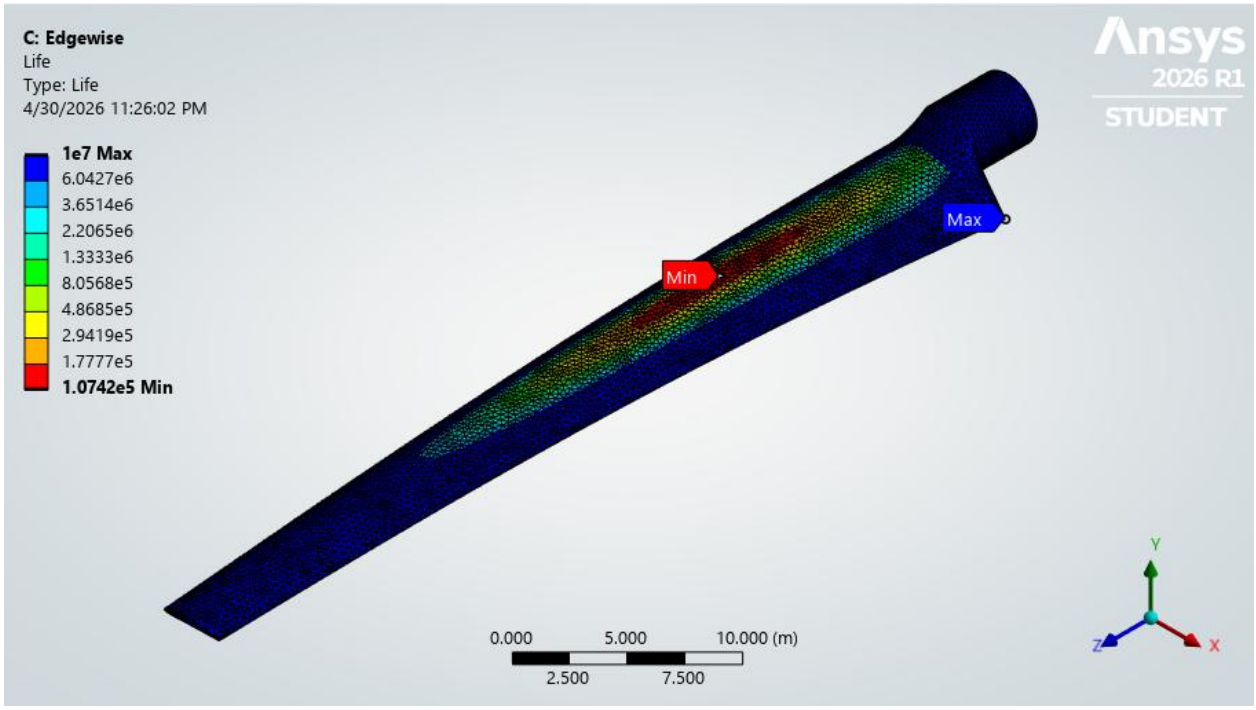


Figure 22d. Fatigue contour of zero-based edgewise bending of the GFRP blade at -40°C

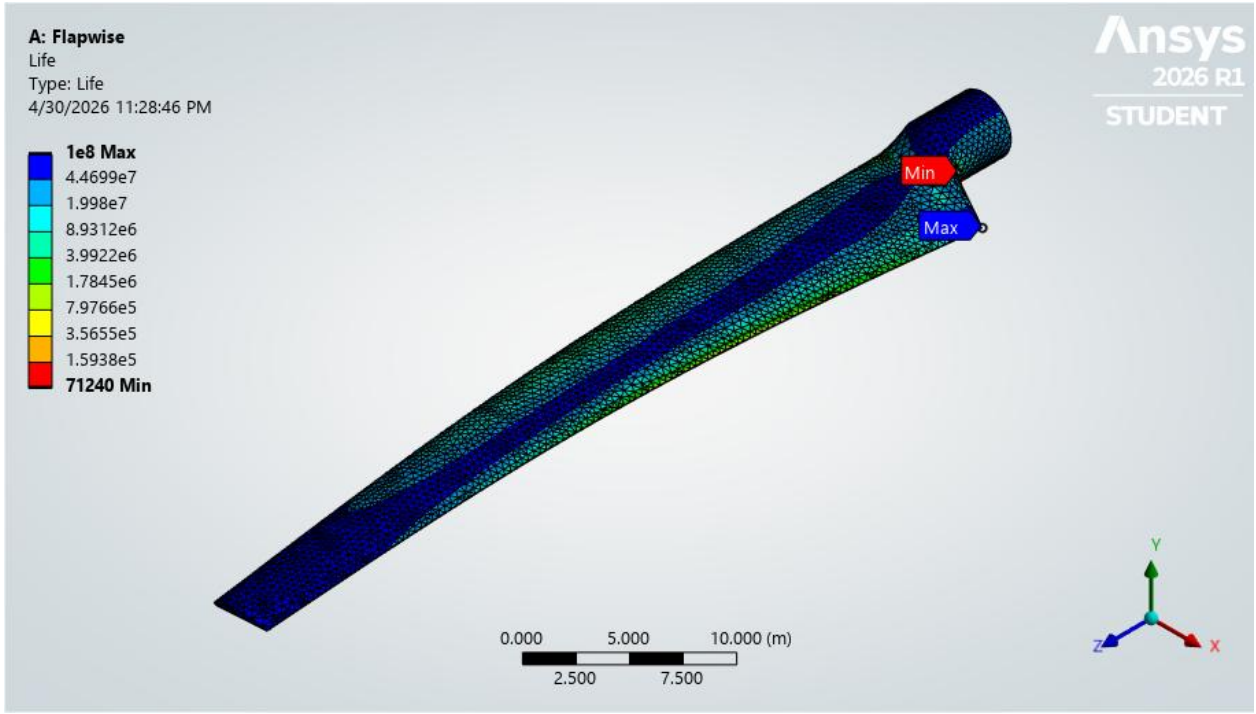


Figure 22e. Fatigue contour of zero-based flapwise bending of the GFRP blade at +60°C

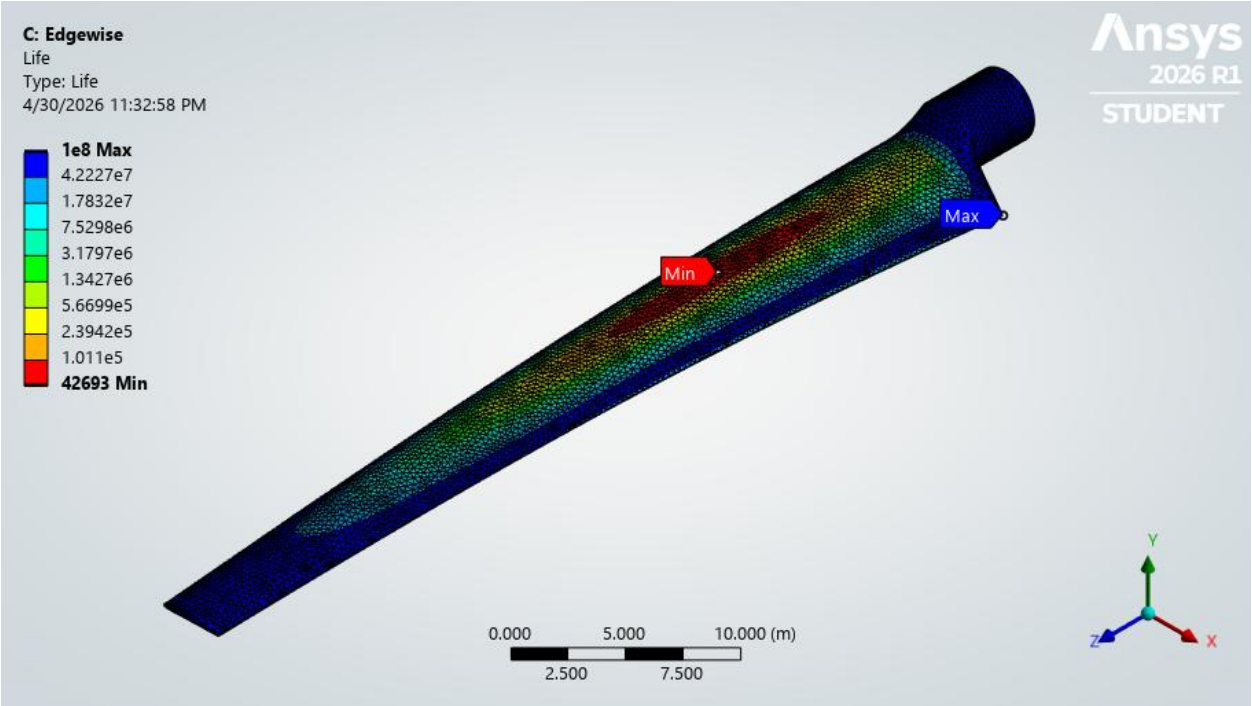


Figure 22f. Fatigue contour of zero-based edgewise bending of the GFRP blade at +60°C

This trend is supported by the published experimental literature. Ou et al. [9] tested unidirectional E-glass/epoxy specimens at six temperatures between -25°C and 100°C and reported a clear increase of tensile strength and Young's modulus when the temperature was decreased; the strength gain was of the order of 15 % between 25°C and -25°C. Jia et al. [10] performed three-point bending tests on CFRP between -100°C and 100°C and observed the same trend, with the flexural strength and the energy absorbed before failure both increasing as the temperature was lowered, until brittle behavior started to dominate below about -60°C. Both studies attribute this effect to the matrix becoming stiffer and the fiber/matrix interface becoming tighter at low temperature [12, 22]. The fatigue improvement obtained in the present simulations is therefore consistent with the data of Ou et al. and Jia et al. and confirms that, in dry conditions, the -40°C Mongolian winter is not by itself a critical situation for a GFRP blade.

This conclusion, however, is valid only as long as ice accretion on the blade is neglected. Reviews by Afzal and Virk [6] and by Hu et al. [8], as well as the numerical study of Jin et al. [30], show that ice accretion at sub-zero temperatures changes the airfoil shape, increases the blade mass, shifts the center of gravity and modifies the load spectrum, and is therefore likely to dominate the cold-climate fatigue behavior. The interaction between the favorable material response at low temperature and the unfavorable aerodynamic effect of ice accretion is one of the open questions that the present study cannot answer.

The reason for the favorable cold-temperature behavior is directly linked to the microstructure of the laminate. GFRP is, in simple terms, a polymer matrix reinforced by glass fibers, which together produce a material that is mechanically superior to either of the constituents. At low temperatures, the polymer matrix becomes stiffer and the bonds between matrix and fibers become tighter, so the laminate can sustain larger flexural loads and absorb more energy before fracture [9, 10]. At higher temperatures, on the contrary, the matrix softens and matrix-fiber debonding occurs more easily, which reduces the fatigue strength of the laminate [11, 12].

4.3. Vibration analysis

4.3.1. Modal analysis

Modal analysis is a standard tool of ANSYS Mechanical. A fixed support was applied at the blade root, and the natural frequencies of the first six modes were extracted. The results are listed in Table 4.

Table 4. Natural frequencies of the first six modes

Mode	Natural frequency, Hz
1	0.27236
2	1.1316
3	1.6516
4	2.8152
5	5.0106
6	5.2904

The values are typical of large multi-megawatt blades. Navadeh et al. [28] computed the natural frequencies of an SNL/MSU blade of similar length using ABAQUS and reported a first flapwise mode close to 0.27 Hz and an edgewise mode close to 1.1 Hz, in good agreement with the first two modes of Table 4. The first natural frequency lies extremely close to the once-per-revolution (1P) excitation of the rotor, equal to $\frac{16.2}{60} = 0.27Hz$ at the maximum rotational speed. This proximity is a known feature of so-called soft-stiff blades and is normally addressed by limiting the operating range of the rotor or by avoiding sustained operation at the rated rotor speed when the wind turbulence has dominant content close to 1P [16, 28].

4.3.2. FFT of the wind speed signal

The procedure described in section 3.3.4 was applied to the wind speed and time series of 15th October 2024 to obtain the one-sided amplitude spectrum of the signal, shown in Fig.23. The spectrum has a clear peak at the lowest non-zero frequency and decays rapidly for higher frequencies, which is the typical shape of an atmospheric wind spectrum where most of the energy is concentrated at low frequencies [16]. The first four natural modes of the blade (0.272, 1.13, 1.65 and 2.82 Hz) all fall well inside the analyzed range below the Nyquist frequency of 5 Hz.

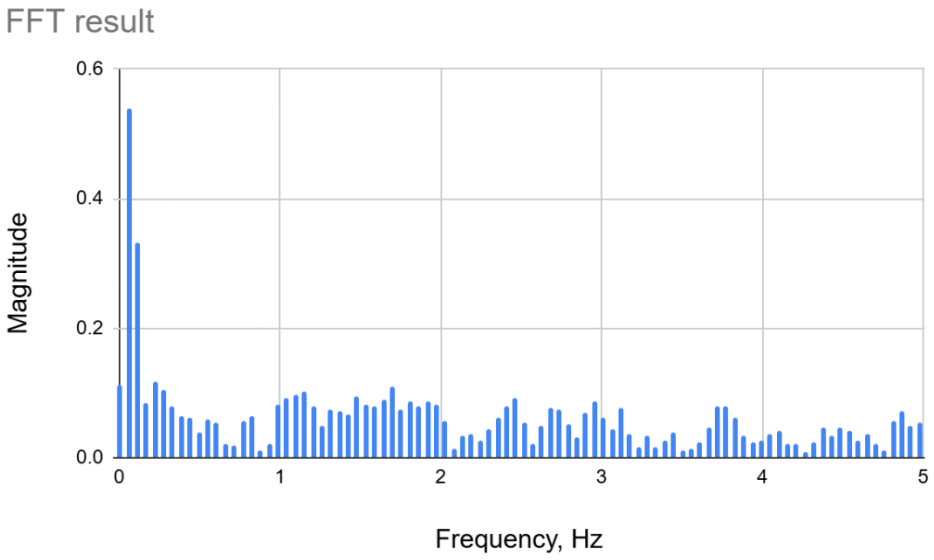


Figure 23. FFT spectrum of the wind speed signal

4.3.3. Resonance risk assessment

The peak of the FFT spectrum has a magnitude of 0.53849 and is located at bin $k = 1$. To check the resonance risk, the bins closest to each natural frequency were inspected. Because part of the energy is spread across the neighboring bins, the maximum magnitude inside the window $(k - 2) < k < (k + 2)$ was extracted and divided by the magnitude of the global peak. The results are summarized in Table 5.

The values obtained for the first four modes are between 16 % and 22 % of the peak. A level of about 20 % is small compared with the global peak, but it is not negligible, and careful monitoring of the blade vibrations and suitable management of the rotational speed are recommended for safe operation.

Table 5. Resonance risk assessment at the bins closest to the natural frequencies

Mode	Natural freq., Hz	Nearest bin, Hz	Bin k	Max magnitude in k ± 2	% of the peak
1	0.27236	0.27322	5	0.11642	21.62
2	1.1316	1.14754	21	0.10241	19.02
3	1.6516	1.63934	30	0.10880	20.20
4	2.8152	2.84153	52	0.08581	15.93

These percentages should not be interpreted as a definitive absence of risk. The wind data was measured at ground level next to the GMIT building and shifted upward to represent rated conditions, so the high-frequency turbulence content normally observed at hub height is most likely under-represented in the spectrum [16]. In addition, ice accretion is known to lower the natural frequencies of a blade because it adds mass without adding stiffness, and in extreme cases the first mode can fall into the 1P excitation band [8, 28]. The conservative recommendation is therefore the same as that given by Navadeh et al. [28]: combine condition monitoring of vibrations with active pitch control to avoid prolonged operation in the resonance range, particularly during winter.

4.4. Limitations of the study and hypotheses

The present work focuses only on the fatigue behavior of the wind turbine blade and necessarily relies on several simplifying assumptions. These assumptions reduce the computational effort to a level that is compatible with a bachelor thesis, but they also create deviations from the real operating conditions of a wind turbine in Mongolia. The most important limitations are summarized below.

First, the study addresses only the structural fatigue of the composite material. Other phenomena that are important under Mongolian conditions, such as ice accretion on the blade [6, 8, 29, 30], leading-edge erosion caused by sand and dust impacts during Gobi storms [7, 19], lightning strikes, and the response of the gearbox, generator and tower, are not modelled. The conclusions therefore apply only to the blade material itself and not to the wind turbine as a complete system.

Second, the wind speed series used as input was collected by the GMIT campus weather station, which is mounted at ground level next to a building. The measured values are too low to be representative of hub-height conditions, and they were therefore shifted upward by a constant offset of 8.9 m/s. This offset places the dataset around the rated wind speed of the GE 1.6-100 turbine, but it does not preserve the full statistical structure of the wind at hub height. Long-term turbulence intensity, gust factors and the extreme

wind events typical of Mongolian sites are not captured. A measurement campaign with anemometers at the actual hub height of 80 to 100 m would be required to remove this limitation.

Third, the blade geometry was downloaded from a public CAD repository and rescaled to match the rotor radius of the reference turbine. The internal structure of a real blade, including the spar caps, the shear webs and the sandwich panels of the trailing edge, is not represented in the simulated geometry. Because most fatigue failures of real blades initiate at the spar cap or at the bonded joints [11, 18, 20], the absence of these features in the model means that the predicted life is an upper bound rather than a realistic estimate.

Fourth, the chord and twist distributions of the original CAD model were unknown and were reconstructed using the Betz-optimal (Schmitz) approach [16, 17]. This approach gives the geometry of an aerodynamically ideal blade, but commercial blades depart from the ideal shape for structural and manufacturing reasons. The simulated aerodynamic loads are therefore optimistic compared with the loads on the real GE 1.6-100 blades.

Fifth, the BEM solver uses two-dimensional polar data extrapolated to plus-minus 180 degrees with the Viterna-Corrigan method [17]. Three-dimensional flow effects, such as spanwise crossflow on stalled airfoils, dynamic inflow and dynamic stall, are therefore not represented. For normal operation between cut-in and rated wind speed the error is small, but it grows in heavily loaded or stalled conditions [16, 17].

Sixth, the structural simulation in ANSYS Mechanical is a sequence of static structural analyses to which the fatigue tool is applied. There is no aero-elastic coupling between the deforming blade and the air flow, and the gravitational reversal due to rotation is included only through the load history rather than through a rotating reference frame. The tower shadow, the wind shear over the rotor disc and the yaw misalignment are all neglected, although they are known contributors to flapwise fatigue [11, 16].

Seventh, the only material property that varies with temperature is the fatigue strength, which was extracted from a digitized S-N graph of the OPTIMAT BLADES OptiDAT database [15]. The static stiffness, the static strength and the thermal expansion coefficient were assumed to be constant. Experimental work on GFRP and CFRP between -40 and 100°C [9, 10] shows that this assumption is acceptable for fiber-dominated properties, but matrix-dominated properties such as transverse strength and interlaminar shear strength may change by 10 to 20 % over the same temperature range.

Eighth, the GFRP material data taken from the ANSYS GRANTA library refers to a printed-circuit-board grade laminate (FR-4) rather than to a wind turbine blade laminate. The fiber volume fraction, the resin chemistry and the lay-up of a real blade differ noticeably, so the absolute stress and life values must be interpreted as indicative rather than as design quantities.

Ninth, the cumulative damage was computed in ANSYS using the linear Palmgren-Miner rule [21]. This rule does not capture load-sequence effects, which are known to be important for composites [12, 23]. More advanced damage models, such as the residual stiffness or progressive damage approach used by Shokrieh and Rafiee [26], were not implemented.

Finally, the resonance risk assessment relies on an assumed sampling frequency of 10 Hz, while the available wind data has a real time step of 60 seconds. The corresponding spectrum can therefore detect the lowest natural frequencies of the blade only in an indicative way, and a higher-rate measurement campaign would be required to confirm the conclusions.

Based on the limitations above and on the literature reviewed in Chapter 2, several hypotheses can be formulated for the operation of horizontal-axis wind turbines under sub-zero or other extreme conditions of the Mongolian climate. These hypotheses are not tested in the present work but provide a starting point for future research.

1. Cold-dense air increases the aerodynamic loads on the blade. The air density at -40°C is approximately 25 % higher than the standard ISA value at sea level. For the same wind speed, the lift and drag forces, and therefore the flapwise and edgewise bending moments, scale with the air density [16, 17]. Pitch and torque control settings tuned for moderate climates may therefore deliver higher than expected fatigue loads in Mongolian winter conditions.
2. Ice accretion is the dominant cold-climate driver of fatigue damage. Even moderate ice layers on the leading edge produce a measurable mass imbalance between the three blades and a strong reduction of the lift coefficient [6, 8, 29, 30]. The combination of a heavier blade, a higher edgewise gravitational moment and an unsteady, partially stalled flow is expected to produce more fatigue damage per revolution than the -40°C dry condition simulated in this work.
3. Repeated freeze-thaw cycles accelerate matrix microcracking. In central Mongolia, daily temperature variations of 20°C or more between day and night are common, especially in spring and autumn. The mismatch between the thermal expansion coefficient of the glass fibers and that of the polymer matrix

produces internal stresses every time the temperature changes. Over many cycles, these stresses are expected to nucleate matrix microcracks and to reduce fatigue life beyond what isothermal cold testing predicts [9, 11, 21].

4. Wind-blown dust and sand erode the blade surface and modify the flow. Dust storms are frequent in southern Mongolia and the Gobi region. Sand particles striking the leading edge progressively remove the gel coat and the outer piles, increase surface roughness and shift the boundary-layer transition forward. The resulting reduction of the lift-to-drag ratio reduces energy capture and produces a more turbulent loading on the structure, which is expected to shorten the fatigue life of the blade [7, 19].
5. The lowest natural frequency of the blade can be excited by 1P and 3P harmonics of the rotor at low wind speeds. The first natural frequency of the GE 1.6-100 blade is 0.272 Hz, very close to the 1P excitation of about 0.27 Hz at 16.2 rpm. Under cold winter conditions, where dense air increases damping but ice accretion increases mass and shifts the natural frequencies downward [8, 28], the safety margin between the rotor harmonics and the first blade mode may be reduced. A targeted aero-elastic study would clarify the practical importance of this effect.
6. CFRP spar caps would extend the fatigue life of the blade in Mongolian winters. The fatigue slope of CFRP is significantly less steep than the slope of GFRP [11, 12], and the experiments of Jia et al. [10] indicate that CFRP retains a large fraction of its flexural strength down to -60°C. A blade in which the spar caps are made of CFRP, while the rest of the structure remains in GFRP, is therefore expected to perform better than an all-GFRP blade in cold-climate sites.
7. Operational practices can compensate for some of the climatic effects. Active pitching strategies that limit the maximum bending moment at low temperatures, periodic de-icing during cold spells and condition monitoring focused on the spar cap region are expected to recover most of the fatigue life lost to icing and freeze-thaw effects [8, 18]. Quantifying these gains requires coupled aero-elastic and probabilistic life simulations.

Verifying or rejecting these hypotheses would require additional measurements (hub height wind data, ice-mass distribution on the blade, daily and seasonal temperature records), more detailed numerical models (icing CFD, full aero-elastic coupling, progressive damage analysis) and dedicated experimental work on representative laminates. The present study, by establishing a baseline for the dry, isothermal fatigue

behavior of the blade, provides a reference point against which future cold-climate studies can be compared.

5. Conclusion

This thesis addressed a question that has direct relevance for the energy future of Mongolia: how does a representative horizontal axis wind turbine blade behave, in fatigue, under the harsh sub-zero conditions of the central Mongolian winter? To answer this question, the work combined three established methods: BEM calculation in Python to compute the flapwise and edgewise root bending moments, a static structural and fatigue analysis in ANSYS Mechanical with three temperature-dependent S-N curves of GFRP extracted from the OPTIMAT BLADES OptiDAT database [15], and a modal analysis combined with a Fast Fourier Transform of the wind speed signal to assess the resonance risk.

The main results can be summarized in four points. First, the BEM solver, with the Betz-optimal (Schmitz) chord and twist distribution, the Viterna-Corrigan extrapolation of the NACA 4412 polar [17, 31] and a control logic that follows the GE 1.6-100 datasheet, produced root bending moments of 1795.812 kNm in flapwise and 294.116 kNm in edgewise direction at rated wind speed. These values lie in the same order of magnitude as those reported by Kong et al. [13] and Shokrieh and Rafiee [26] for blades of comparable size and confirm the consistency of the calculation. Second, the fatigue analysis showed that the laminate can sustain more than one hundred million cycles at the maximum flapwise moment, with safety factors larger than 15 at room temperature. Third, the simulations at -40°C, room temperature and +60°C reproduce the trend reported in the experimental work of Ou et al. [9] and Jia et al. [10]: a smaller fraction of the blade reaches the failure threshold at -40°C than at higher temperatures, which suggests that, in dry conditions, the cold of a Mongolian winter is not by itself a critical factor. Fourth, the modal analysis returned natural frequencies very close to those reported by Navadeh et al. [28], and the FFT of the wind speed signal showed that the magnitudes at the natural-frequency bins remain below 22 % of the spectral peak, indicating a moderate but non-negligible resonance risk.

These findings should be read as a baseline rather than as a complete picture of blade behavior in Mongolia. The study deliberately ignores ice accretion, freeze-thaw cycles, dust erosion, lightning, the internal structure of the blade and the coupling between

aerodynamics and elasticity. As shown in section 5.1, every one of these simplifications removes an effect that is known to be important in the real Mongolian winter. The literature reviewed in chapter 2 makes it clear that ice accretion alone can reduce the annual energy production by 5 to 20 % [6] and modify the natural frequencies of the blade [8, 28], that dust storms in the Gobi region progressively erode the leading edge [7], and that freeze-thaw cycles can nucleate matrix microcracks even in the absence of mechanical loading [9, 11, 21]. The very high safety factor obtained at room temperature should therefore be interpreted as an upper bound and as the starting point for more refined studies.

Mongolia has one of the highest wind resources in Asia, with an estimated potential of more than one terawatt of installed capacity. Realizing this potential is essential if the country wants to reduce its dependence on coal-fired electricity and air pollution caused by it, particularly in Ulaanbaatar during winter, and to meet its commitments under the Paris Agreement. The path to a green future therefore goes through wind turbines that operate reliably in the very specific climate of the country: extreme cold, large diurnal temperature swings, frequent dust storms and occasional ice events. The correct determination of how a horizontal axis wind turbine behaves at the freezing temperatures of Mongolia is, for this reason, not an optional refinement but a necessary step. Without it, design margins must be conservatively large, energy yield is sacrificed and maintenance costs are difficult to predict.

Several lines of further work follow naturally from the limitations and from the hypotheses formulated in chapter 5. The most urgent are a measurement campaign at hub height to obtain realistic wind data, an icing CFD study to quantify the additional aerodynamic and structural loads under typical Mongolian winter conditions [8, 29, 30, 32], a progressive damage analysis on a more realistic internal blade structure [23, 26], and dedicated coupon tests on representative GFRP and CFRP laminates after several hundred freeze-thaw cycles [9, 10]. Combining these results with the baseline obtained in this thesis would make it possible to predict, with adequate confidence, the fatigue life of a multi-megawatt blade installed in Sergelen or in any other site in Mongolia.

In summary, the present thesis demonstrates that a careful combination of BEM calculation, finite element fatigue analysis and basic modal/FFT assessment can capture the dry, isothermal fatigue response of a HAWT blade at sub-zero temperatures. The results are encouraging in that the cold of a Mongolian winter alone does not appear to threaten the structural integrity of a GFRP blade. The results are also a reminder that the real Mongolian winter is far more complex than the dry isothermal case studied here,

and that closing the remaining gap is a prerequisite for the responsible deployment of large-scale wind energy in the country. In this sense, the work establishes a baseline that future studies can build on and contributes a small but concrete step toward a green future for Mongolia.

6. References

[1] United Nations. What is climate change? [Internet]. New York: United Nations; 2025 [cited 2026 May 1]. Available from: https://www.un.org/en/climatechange/what-is-climate-change

[2] Wind power in Germany [Internet]. Wikipedia; 2024 [cited 2026 May 1]. Available from: https://en.wikipedia.org/wiki/Wind_power_in_Germany

[3] Energy in Mongolia [Internet]. Wikipedia; 2020 [cited 2026 May 1]. Available from: https://en.wikipedia.org/wiki/Energy_in_Mongolia

[4] Mining in Mongolia [Internet]. Wikipedia; 2022 [cited 2026 May 1]. Available from: https://en.wikipedia.org/wiki/Mining_in_Mongolia

[5] Global Wind Atlas [Internet]. Roskilde: Technical University of Denmark; 2024 [cited 2026 May 1]. Available from: https://globalwindatlas.info/en

[6] Afzal F, Virk MS. Review of icing effects on wind turbine in cold regions. E3S Web Conf. 2018;72:01007.

[7] Douvi E, Douvi DC. Aerodynamic characteristics of wind turbines operating under hazard environmental conditions: a review. Energies. 2023;16(24):7681.

[8] Hu H, Gao L, Liu Y. Wind turbine icing physics and anti-/de-icing technology. London: Academic Press; 2022.

[9] Ou Y, Zhu D, Zhang H, Huang L, Yao Y, Li G, et al. Mechanical characterization of the tensile properties of glass fiber and its reinforced polymer (GFRP) composite under varying strain rates and temperatures. Polymers. 2016;8(5):196.

[10] Jia Z, Li T, Chiang FP, Wang L. An experimental investigation of the temperature effect on the mechanics of carbon fiber reinforced polymer composites. Compos Sci Technol. 2018;154:53-63.

[11] Brondsted P, Nijssen RPL, Goutianos S, editors. Advances in wind turbine blade design and materials. 2nd ed. Cambridge: Woodhead Publishing; 2023.

[12] Nijssen RPL. Fatigue life prediction and strength degradation of wind turbine rotor blade composites [PhD thesis]. Delft: Delft University of Technology; 2006.

[13] Kong C, Bang J, Sugiyama Y. Structural investigation of composite wind turbine blade considering various load cases and fatigue life. Energy. 2005;30(11-12):2101-14.

[14] OPTIMAT BLADES Consortium. Reliable optimal use of materials for wind turbine rotor blades - final report. Petten: Energy Research Centre of the Netherlands (ECN); 2006.

[15] Vallons KA. Databases for fatigue analysis in composite materials. InFatigue of Textile Composites 2015 Jan 1 (pp. 75-82). Woodhead Publishing.

[16] Burton T, Jenkins N, Bossanyi E, Sharpe D, Graham M. Wind energy handbook. 3rd ed. Chichester: John Wiley & Sons; 2021.

[17] Schaffarczyk AP. Introduction to wind turbine aerodynamics. 2nd ed. Berlin: Springer; 2024.

[18] Olabi AG, Wilberforce T, Elsaid K, Sayed ET, Salameh T, Abdelkareem MA, et al. A review on failure modes of wind turbine components. Energies. 2021;14(17):5241.

[19] Katsaprakakis DA, Papadakis N, Ntintakis I. A comprehensive analysis of wind turbine blade damage. Energies. 2021;14(18):5974.

[20] Chou JS, Chiu CK, Huang IK, Chi KN. Failure analysis of wind turbine blade under critical wind loads. Eng Fail Anal. 2013;27:99-118.

[21] Dowling NE, Kampe SL, Kral MV. Mechanical behavior of materials. 5th ed., global ed. Harlow: Pearson; 2019.

[22] Douvi DC, Douvi E, Margaris DP. The operation of a three-bladed horizontal axis wind turbine under hailstorm conditions - a computational study focused on aerodynamic performance. Inventions. 2022;7(1):2.

[23] Colombo C, Libonati F, Vergani L. Fatigue damage in GFRP. Int J Struct Integr. 2012;3(4):424-40.

[24] Kong C, Kim T, Han D, Sugiyama Y. Investigation of fatigue life for a medium scale composite wind turbine blade. Int J Fatigue. 2006;28(10):1382-8.

[25] Tawade SV, Todkar SB, Hade AS. Fatigue life optimization of wind turbine blade. Int J Res Eng Technol. 2014;3(Special Issue 3):320-4.

[26] Shokrieh MM, Rafiee R. Simulation of fatigue failure in a full composite wind turbine blade. Compos Struct. 2006;74(3):332-42.

[27] Mandell JF, Samborsky DD. SNL/MSU/DOE composite material fatigue database: test methods, materials, and analysis. Albuquerque (NM): Sandia National Laboratories; 2019.

[28] Navadeh N, Goroshko I, Zhuk Y, Etminan Moghadam F, Soleiman Fallah A. Finite element analysis of wind turbine blade vibrations. Vibration. 2021;4(2):310-22.

[29] Bhatia D, Al Wahaibi A. A numerical investigation into the impact of icing on the aerodynamic performance of aerofoils. IOP Conf Ser Mater Sci Eng. 2020;831:012001.

[30] Jin J, Virk MS, Hu Q, Jiang X. Study of ice accretion on horizontal axis wind turbine blade using 2D and 3D numerical approach. IEEE Access. 2020;8:166236-45.

[31] Ockfen AE, Matveev KI. Aerodynamic characteristics of NACA 4412 airfoil section with flap in extreme ground effect. Int J Nav Archit Ocean Eng. 2009;1(1):1-12.

[32] Ozgen S, Saribel EB. Airfoil icing prediction with improved roughness model. J Phys Conf Ser. 2024;2767:052020.

Appendix

Full datasheet of the wind turbine model

GE Vernova 1.6 - 100	
Rated power	1600 kW
Cut-in speed	3.5 m/s
Rated speed	11 m/s
Cut-out speed	25 m/s
Rotor	
Diameter	100 m
Swept area	7854 m^2
Number of Blades	3
Rotor speed, max	16.2 RPM
Tip speed	85 m/s
Type	48.7
Material	GFK
Power density 1	203.7 W/m^2
Power density 2	4.9 m^2/kW
Gearbox	
Type	Spur/planetary
Stages	3
Ratio	1:115
Generator	
Type	Double Fed Asyn
Number	1
Voltage	690 V
Grid connection	IGBT
Grid frequency	50-60 Hz
Tower	
Hub height	80/100 m
Type	Steel tube
Shape	Conical
Corrosion protection	painted
Weight	
Nacelle	65 t
Miscellaneous	
Onshore	Yes
Offshore	No

The BEM theory calculation data

Time_s	WindSpeed_m/s	Pitch_deg	RotorSpeed_RPM	Power_kW	Thrust_kN	Torque_kNm	Mflap_kNm	Medge_kNm
12	8.9	0	13.135	929.155	128.377	675.526	1197.259	196.085
72	10.3	0	15.201	1440.223	171.942	904.766	1603.55	262.627
132	9.6	0	14.168	1166.089	149.366	785.967	1392.998	228.143
192	10.5	0	15.496	1525.759	178.685	940.244	1666.428	272.925
252	10.2	0	15.053	1398.681	168.62	887.283	1572.564	257.553
312	10.4	0	15.348	1482.58	175.297	922.42	1634.838	267.752
372	10.6	0	15.643	1569.769	182.104	958.238	1698.321	278.149
432	10.8	0	15.939	1660.31	189.041	994.739	1763.013	288.744
492	10.1	0	14.906	1357.945	165.33	869.971	1541.881	252.527
552	10.1	0	14.906	1357.945	165.33	869.971	1541.881	252.527
612	10.6	0	15.643	1569.769	182.104	958.238	1698.321	278.149
672	10.5	0	15.496	1525.759	178.685	940.244	1666.428	272.925

732	10.6	0	15.643	1569.769	182.104	958.238	1698.321	278.149
792	10.7	0	15.791	1614.616	185.556	976.404	1730.516	283.422
852	10.6	0	15.643	1569.769	182.104	958.238	1698.321	278.149
912	10.6	0	15.643	1569.769	182.104	958.238	1698.321	278.149
972	10	0	14.758	1318.008	162.072	852.829	1511.499	247.551
1032	9.7	0	14.315	1202.91	152.494	802.427	1422.17	232.921
1092	10	0	14.758	1318.008	162.072	852.829	1511.499	247.551
1152	10.4	0	15.348	1482.58	175.297	922.42	1634.838	267.752
1212	10.1	0	14.906	1357.945	165.33	869.971	1541.881	252.527
1272	10.3	0	15.201	1440.223	171.942	904.766	1603.55	262.627
1332	10.6	0	15.643	1569.769	182.104	958.238	1698.321	278.149
1392	10.1	0	14.906	1357.945	165.33	869.971	1541.881	252.527
1452	10	0	14.758	1318.008	162.072	852.829	1511.499	247.551
1512	9.9	0	14.61	1278.862	158.847	835.857	1481.421	242.625
1572	10.3	0	15.201	1440.223	171.942	904.766	1603.55	262.627
1632	10.3	0	15.201	1440.223	171.942	904.766	1603.55	262.627
1692	10.1	0	14.906	1357.945	165.33	869.971	1541.881	252.527
1752	10.3	0	15.201	1440.223	171.942	904.766	1603.55	262.627
1812	10.3	0	15.201	1440.223	171.942	904.766	1603.55	262.627
1872	10	0	14.758	1318.008	162.072	852.829	1511.499	247.551
1932	10.8	0	15.939	1660.31	189.041	994.739	1763.013	288.744
1992	10.6	0	15.643	1569.769	182.104	958.238	1698.321	278.149
2052	10.9	0	16.086	1706.859	192.558	1013.246	1795.812	294.116
2112	10.3	0	15.201	1440.223	171.942	904.766	1603.55	262.627
2172	10.3	0	15.201	1440.223	171.942	904.766	1603.55	262.627
2232	10.1	0	14.906	1357.945	165.33	869.971	1541.881	252.527
2292	10.8	0	15.939	1660.31	189.041	994.739	1763.013	288.744
2352	10	0	14.758	1318.008	162.072	852.829	1511.499	247.551
2412	10.5	0	15.496	1525.759	178.685	940.244	1666.428	272.925
2472	10.1	0	14.906	1357.945	165.33	869.971	1541.881	252.527
2532	10.3	0	15.201	1440.223	171.942	904.766	1603.55	262.627
2592	10	0	14.758	1318.008	162.072	852.829	1511.499	247.551
2652	9.9	0	14.61	1278.862	158.847	835.857	1481.421	242.625
2712	10.1	0	14.906	1357.945	165.33	869.971	1541.881	252.527
2772	10.2	0	15.053	1398.681	168.62	887.283	1572.564	257.553
2832	10.1	0	14.906	1357.945	165.33	869.971	1541.881	252.527
2892	10.4	0	15.348	1482.58	175.297	922.42	1634.838	267.752
2952	10.6	0	15.643	1569.769	182.104	958.238	1698.321	278.149
3012	10.6	0	15.643	1569.769	182.104	958.238	1698.321	278.149
3072	10.3	0	15.201	1440.223	171.942	904.766	1603.55	262.627
3132	10	0	14.758	1318.008	162.072	852.829	1511.499	247.551
3192	10	0	14.758	1318.008	162.072	852.829	1511.499	247.551
3252	10	0	14.758	1318.008	162.072	852.829	1511.499	247.551
3312	9.9	0	14.61	1278.862	158.847	835.857	1481.421	242.625
3372	9.8	0	14.463	1240.499	155.654	819.057	1451.644	237.748
3432	9.7	0	14.315	1202.91	152.494	802.427	1422.17	232.921
3492	9.6	0	14.168	1166.089	149.366	785.967	1392.998	228.143
3552	9.6	0	14.168	1166.089	149.366	785.967	1392.998	228.143
3612	9.6	0	14.168	1166.089	149.366	785.967	1392.998	228.143
3672	9.6	0	14.168	1166.089	149.366	785.967	1392.998	228.143
3732	9.9	0	14.61	1278.862	158.847	835.857	1481.421	242.625
3792	9.7	0	14.315	1202.91	152.494	802.427	1422.17	232.921

3852	9.4	0	13.873	1094.716	143.207	753.559	1335.561	218.736
3912	9.7	0	14.315	1202.91	152.494	802.427	1422.17	232.921
3972	9.3	0	13.725	1060.149	140.176	737.612	1307.296	214.107
4032	9.5	0	14.02	1130.027	146.27	769.678	1364.128	223.415
4092	10	0	14.758	1318.008	162.072	852.829	1511.499	247.551
4152	10	0	14.758	1318.008	162.072	852.829	1511.499	247.551
4212	9.7	0	14.315	1202.91	152.494	802.427	1422.17	232.921
4272	10	0	14.758	1318.008	162.072	852.829	1511.499	247.551
4332	9.7	0	14.315	1202.91	152.494	802.427	1422.17	232.921
4392	9.9	0	14.61	1278.862	158.847	835.857	1481.421	242.625
4452	9.9	0	14.61	1278.862	158.847	835.857	1481.421	242.625
4512	9.7	0	14.315	1202.91	152.494	802.427	1422.17	232.921
4572	9	0	13.282	960.828	131.278	690.791	1224.315	200.517
4632	10	0	14.758	1318.008	162.072	852.829	1511.499	247.551
4692	9.5	0	14.02	1130.027	146.27	769.678	1364.128	223.415
4752	9.3	0	13.725	1060.149	140.176	737.612	1307.296	214.107
4812	9.3	0	13.725	1060.149	140.176	737.612	1307.296	214.107
4872	9.8	0	14.463	1240.499	155.654	819.057	1451.644	237.748
4932	9.6	0	14.168	1166.089	149.366	785.967	1392.998	228.143
4992	9.8	0	14.463	1240.499	155.654	819.057	1451.644	237.748
5052	10.2	0	15.053	1398.681	168.62	887.283	1572.564	257.553
5112	9.8	0	14.463	1240.499	155.654	819.057	1451.644	237.748
5172	10.5	0	15.496	1525.759	178.685	940.244	1666.428	272.925
5232	10.3	0	15.201	1440.223	171.942	904.766	1603.55	262.627
5292	10.8	0	15.939	1660.31	189.041	994.739	1763.013	288.744
5352	10.5	0	15.496	1525.759	178.685	940.244	1666.428	272.925
5412	10.9	0	16.086	1706.859	192.558	1013.246	1795.812	294.116
5472	10.6	0	15.643	1569.769	182.104	958.238	1698.321	278.149
5532	10.7	0	15.791	1614.616	185.556	976.404	1730.516	283.422
5592	10.7	0	15.791	1614.616	185.556	976.404	1730.516	283.422
5652	11.5	3.281	16.2	1600	163.591	943.168	1473.872	271.861
5712	10.5	0	15.496	1525.759	178.685	940.244	1666.428	272.925
5772	10.7	0	15.791	1614.616	185.556	976.404	1730.516	283.422
5832	11.3	2.717	16.2	1599.657	167.514	942.938	1522.49	272.253
5892	11.3	2.717	16.2	1599.657	167.514	942.938	1522.49	272.253
5952	10.4	0	15.348	1482.58	175.297	922.42	1634.838	267.752
6012	10	0	14.758	1318.008	162.072	852.829	1511.499	247.551
6072	11.3	2.717	16.2	1599.657	167.514	942.938	1522.49	272.253
6132	12.3	5.315	16.2	1600	150.22	943.156	1303.506	269.867
6192	11.2	2.427	16.2	1599.086	169.551	942.601	1547.608	272.379
6252	10.5	0	15.496	1525.759	178.685	940.244	1666.428	272.925
6312	10.5	0	15.496	1525.759	178.685	940.244	1666.428	272.925
6372	10.3	0	15.201	1440.223	171.942	904.766	1603.55	262.627
6432	10.6	0	15.643	1569.769	182.104	958.238	1698.321	278.149
6492	10.3	0	15.201	1440.223	171.942	904.766	1603.55	262.627
6552	11.3	2.717	16.2	1599.657	167.514	942.938	1522.49	272.253
6612	11.9	4.341	16.2	1599.663	156.434	942.942	1383.742	270.82
6672	10.9	0	16.086	1706.859	192.558	1013.246	1795.812	294.116
6732	10.8	0	15.939	1660.31	189.041	994.739	1763.013	288.744
6792	10.9	0	16.086	1706.859	192.558	1013.246	1795.812	294.116
6852	10.8	0	15.939	1660.31	189.041	994.739	1763.013	288.744
6912	11.4	3.008	16.2	1599.308	165.45	942.732	1497.124	271.963

6972	11.1	2.119	16.2	1599.419	171.79	942.798	1574.812	272.658
7032	10.6	0	15.643	1569.769	182.104	958.238	1698.321	278.149
7092	11.1	2.119	16.2	1599.419	171.79	942.798	1574.812	272.658
7152	10.7	0	15.791	1614.616	185.556	976.404	1730.516	283.422
7212	10.6	0	15.643	1569.769	182.104	958.238	1698.321	278.149
7272	13.1	7.092	16.2	1599.673	139.598	942.947	1161.835	267.662
7332	12.4	5.554	16.2	1599.332	148.697	942.746	1283.844	269.487
7392	14.2	9.229	16.2	1600	128.302	943.506	1003.928	264.896
7452	11.3	2.717	16.2	1599.657	167.514	942.938	1522.49	272.253
7512	10.4	0	15.348	1482.58	175.297	922.42	1634.838	267.752
7572	10.4	0	15.348	1482.58	175.297	922.42	1634.838	267.752
7632	10.9	0	16.086	1706.859	192.558	1013.246	1795.812	294.116
7692	13.1	7.092	16.2	1599.673	139.598	942.947	1161.835	267.662
7752	13.2	7.297	16.2	1600	138.468	943.207	1146.16	267.46
7812	10.5	0	15.496	1525.759	178.685	940.244	1666.428	272.925
7872	12.4	5.554	16.2	1599.332	148.697	942.746	1283.844	269.487
7932	12.3	5.315	16.2	1600	150.22	943.156	1303.506	269.867
7992	11.8	4.084	16.2	1599.736	158.13	942.985	1405.302	271.082
8052	11.3	2.717	16.2	1599.657	167.514	942.938	1522.49	272.253
8112	12.3	5.315	16.2	1600	150.22	943.156	1303.506	269.867
8172	10.9	0	16.086	1706.859	192.558	1013.246	1795.812	294.116
8232	10.5	0	15.496	1525.759	178.685	940.244	1666.428	272.925
8292	13.2	7.297	16.2	1600	138.468	943.207	1146.16	267.46
8352	16.7	13.501	16.2	1599.681	110.024	942.953	720.641	256.141
8412	10.9	0	16.086	1706.859	192.558	1013.246	1795.812	294.116
8472	11	1.794	16.2	1600	174.213	943.343	1603.957	273.04
8532	10.8	0	15.939	1660.31	189.041	994.739	1763.013	288.744
8592	11	1.794	16.2	1600	174.213	943.343	1603.957	273.04
8652	10.5	0	15.496	1525.759	178.685	940.244	1666.428	272.925
8712	12.7	6.229	16.2	1599.795	144.609	943.02	1229.464	268.774
8772	12	4.589	16.2	1600	154.842	943.184	1363.258	270.641
8832	11.2	2.427	16.2	1599.086	169.551	942.601	1547.608	272.379
8892	12.2	5.076	16.2	1600	151.733	943.27	1323.116	270.158
8952	11.9	4.341	16.2	1599.663	156.434	942.942	1383.742	270.82
9012	13.3	7.502	16.2	1599.855	137.308	943.055	1130.095	267.13
9072	11	1.794	16.2	1600	174.213	943.343	1603.957	273.04
9132	11.1	2.119	16.2	1599.419	171.79	942.798	1574.812	272.658
9192	11.3	2.717	16.2	1599.657	167.514	942.938	1522.49	272.253
9252	10.5	0	15.496	1525.759	178.685	940.244	1666.428	272.925
9312	13.2	7.297	16.2	1600	138.468	943.207	1146.16	267.46
9372	11.2	2.427	16.2	1599.086	169.551	942.601	1547.608	272.379
9432	11	1.794	16.2	1600	174.213	943.343	1603.957	273.04
9492	10.9	0	16.086	1706.859	192.558	1013.246	1795.812	294.116
9552	11.7	3.828	16.2	1599.171	159.811	942.652	1426.753	271.23
9612	10.9	0	16.086	1706.859	192.558	1013.246	1795.812	294.116
9672	13.7	8.289	16.2	1600	133.112	943.453	1070.707	266.088
9732	13.9	8.673	16.2	1600	131.141	943.469	1042.656	265.503
9792	12.3	5.315	16.2	1600	150.22	943.156	1303.506	269.867
9852	13	6.879	16.2	1600	140.835	943.215	1178.546	268.019
9912	11.1	2.119	16.2	1599.419	171.79	942.798	1574.812	272.658
9972	11.1	2.119	16.2	1599.419	171.79	942.798	1574.812	272.658
10032	11	1.794	16.2	1600	174.213	943.343	1603.957	273.04

10092	12.5	5.776	16.2	1600	147.408	943.488	1266.56	269.447
10152	11.2	2.427	16.2	1599.086	169.551	942.601	1547.608	272.379
10212	13.3	7.502	16.2	1599.855	137.308	943.055	1130.095	267.13
10272	14.4	9.604	16.2	1599.589	126.455	942.898	977.138	264.074
10332	13.8	8.485	16.2	1599.914	132.063	943.09	1056.021	265.685
10392	12.6	6.007	16.2	1599.84	145.956	943.046	1247.503	269.05
10452	11.1	2.119	16.2	1599.419	171.79	942.798	1574.812	272.658
10512	10.3	0	15.201	1440.223	171.942	904.766	1603.55	262.627
10572	10.6	0	15.643	1569.769	182.104	958.238	1698.321	278.149
10632	10.9	0	16.086	1706.859	192.558	1013.246	1795.812	294.116
10692	12.8	6.443	16.2	1600	143.389	943.534	1212.776	268.657
10752	13.5	7.896	16.2	1600	135.213	943.665	1100.304	266.735
10812	12.5	5.776	16.2	1600	147.408	943.488	1266.56	269.447
10872	12.5	5.776	16.2	1600	147.408	943.488	1266.56	269.447
10932	10.9	0	16.086	1706.859	192.558	1013.246	1795.812	294.116